MICROARRAY PROBE DEVELOPMENT FOR THE IMAGING OF HUMAN TUMORS

A Honors Thesis Presented in Partial Fulfillment of the Requirements for Graduation with Distinction in the Department of Mechanical and Aerospace Engineering at The Ohio State University

Ryan Snodgrass

3/31/2014

Defense Committee Member	Approval
Dr. Shaurya Prakash, Advisor	_____
Dr. Vishwanath Subramanium	_____

ABSTRACT

Tissues of different composition or type can be distinguished due to differences in electrical impedance, measured using electrochemical impedance spectroscopy (EIS). Real-time EIS measurements presented as tissue images can potentially help surgeons identify the surgical margin of human tumors during organ resection. Sufficient surgical margin is important for patient survival rates but is presently estimated by non-quantitative methods such as visual inspection and physical palpation, and is verified for accuracy only post-surgery. Tumor images produced by existing impedance devices require the use of cumbersome stages and extensive supporting electronics to generate only coarse images of tumors in timespans of over 30 minutes. Consequently, existing impedance devices are impractical as real-time surgical tools for the verification of surgical margins. A rapid, non-translational electrode array probe is in development that will allow for the real-time imaging of human tumors, especially at the tumor/non-tumor interface. The newly developed measurement device has shown that physical probe translation can be eliminated through the use of a microarray as a probe and a multiplexing circuit as an electrode-switching mechanism. The custom designed probe and multiplexer enables successful imaging of tissue heterogeneity as demonstrated both in tissue phantoms and excised human liver tissue with metastatic colorectal cancer. Tissue images made from 26 serial EIS measurements can now be generated in just over two minutes. Additionally, the spatial resolution of the probe is now reaching almost 1 mm, not currently achieved by any other tissue electrical-characterization method in real-time. Therefore, the microarray probe can define a precise surgical margin in a time more acceptable for an active surgical environment.

ACKNOWLEDGEMENTS

First and foremost, I would like to thank Dr. Shaurya Prakash for all of his advice, motivation, and leadership throughout my work on this research project, in addition to many enjoyable discussions concerning both work and life. I would also like to thank Karen Bellman and Ben Shurtz for being great peers and mentors throughout the duration of my research. Additionally, I would like to thank everyone else who made such a collaborative project possible: Emily Sequin, for her assistance during liver sample measurements; Dr. Vishwanath Subramaniam, for his collaboration, support, and knowledge; doctors Charles Hitchcock, Shawnn Nichols, and Edward Martin for their assistance in sample retrieval; and the rest of the Microsystems and Nanosystems Laboratory, who have made work fun and who have been part of many great discussions: both recreational and scientific.

DEDICATION

To my parents, grandparents, and siblings: for their selfless support.

TABLE OF CONTENTS

LIST OF FIGURES

LIST OF TABLES

CHAPTER 1. INTRODUCTION

The following thesis details the design, construction, and testing of a measurement device to be used during the resection of colorectal cancer. There is currently a need for an automated measurement device that could provide real-time identification of the tumor/non-tumor interface in order to assist surgeons in the identification of the surgical margin. The device to be detailed must be able to provide surgical feedback in real-time, and it must be able to define a precise surgical margin. It is also essential that the device has a small form-factor, as the eventual product must be able to be easily integrated as a surgical tool with little interference to existing clinical settings and practices.

1.1 Importance of the Surgical Margin

Tumor resection is the surgical removal of portions of the organ(s) bearing tumor tissue. The primary and preferred method for treatment of primary and metastatic cancers, including those in hepatic tissue, is through tumor resection (Haemmerich et al., 2009). A current challenge for surgeons during organ resection surgeries is in the identification of the surgical margin, i.e. the amount of normal tissue that is removed with tumors in an attempt to assure that the patient is free of all tumors. The size of the surgical margin is important to patient survival rates (Cady, et al., 1998). A particular study found that five years after colorectal tumor resection there was a 63.8% survival rate for patients with sufficient surgical margin versus a 17.1% survival rate for patients with insufficient surgical margin (Pawlik et al., 2005). The surgical margin is presently estimated by a surgeon's sight, touch and palpation, and experience in cancer treatment. Furthermore, verification of margins is only confirmed post-surgery through pathology, when it is too late to give real-time feedback to the surgeon. Therefore, the Prakash group has been developing a tool that will allow for precise, real-time identification of the surgical margin. The

tool is hoped to be implemented into the hands of a surgeon, allowing him/her to quantitatively locate a sufficient surgical margin and thus provide direct benefits for surgical cancer treatment of patients undergoing tumor resection surgeries.

To develop such a surgical tool, the group has exploited the knowledge that tumor and normal tissues usually differ in electrical conductivity as estimated through electrical or electrochemical impedance (EIS). One of the first studies that compared electrical conductivities of tumor/non-tumor human tissue determined that tumor in the breast was more electrically conductive than the surrounding normal tissue (Fricke & Morse, 1926). Studies have determined that a similar trend exists in human liver tissue (liver tissue will be the focus of this study), with the tumor tissue being more conductive than the normal liver tissue (Haemmerich et al., 2009). Since it is known that tumor tissue in the human liver is more conductive than normal human liver tissue, and because impedance and conductivity are inversely related, it can be concluded that tumor tissue should exhibit lower electrical impedance values in comparison to electrical impedance values in normal tissue:

$$Z_{tumor} < Z_{normal} \tag{1}$$

Therefore, if other experimental parameters are kept constant (e.g., sample thickness, wetness or hydration levels, etc.), impedance values collected using EIS can be used to identify tumor tissue amongst normal tissue in the human liver. Much of the work done by the Prakash group, as well as the focus of this thesis, has been in automating the process of collecting EIS measurements in locations across the surface of a tissue. Multiple EIS measurements allow for the generation of an impedance map: an image contrasting impedance values that enables the precise identification of tumor location. First, however, it is important to discuss the operation of a single EIS measurement so that the design of a measurement automation device can be fully explained.

1.2 Single EIS Measurement Analysis

To quantify and measure tissue impedance, electrical signals need to be provided and the tissue electrical response recorded. For this purpose, the Gamry Reference 600 potentiostat was used. The potentiostat was used in galvanostatic mode, meaning that it input a constant amplitude (AC) electrical current:

$$i(\omega) = i_0 \sin(\omega t) \tag{2}$$

(Equations 2 through 8 were adapted from Gamry Instruments Incorporated.) The angular frequency of the current, ω, was varied throughout individual measurements, with the corresponding linear frequency range being 100 Hz – 1 MHz with i_o being 30 μA RMS with 10 points per decade in the recorded response. The frequency range was based off of previous work, which performed experiments between 100 Hz and 1 MHz (Haemmerich et al., 2009). However, most experiments in this thesis were kept between 1 kHz and 100 kHz, for reasons to be discussed in Chapter 3. The current was injected using two electrodes, called the working and counter electrodes. Then, using two separate electrodes, called the working sense and reference electrodes, a frequency-dependent voltage was measured as:

$$V(\omega) = V_0 \sin(\omega t + \theta) \tag{3}$$

The measured voltage returns at the same frequency as the input signal, but with a phase shift, θ. The impedance of the tissue can then be calculated as the ratio of the measured voltage over the injected current.

$$Z(\omega) = V(\omega)/I(\omega) \tag{4}$$

Or

$$Z(\omega) = Z_0 \frac{\sin(\omega t)}{\sin(\omega t + \theta)} \tag{5}$$

Using Euler's formula, with j representing the complex number-set:

$$\exp(j\theta) = \cos(\theta) + jsin(\theta) \tag{6}$$

So that

$$Z(\omega) = Z_0 \frac{\exp(j\omega t)}{\exp(j\omega t + \theta)} \tag{7}$$

Finally, the impedance can be represented as real and imaginary parts:

$$Z(\omega) = Z_0(\cos\theta - jsin\theta) \tag{8}$$

For tissue measurements performed in this thesis, the modulus of the impedance (a scalar, equation 9) will usually be used for analysis, although phase and the DC part of the measured current were also recorded.

$$Z_{modulus} = \sqrt{{Z_{real}}^2 + {Z_{imaginary}}^2} \tag{9}$$

The impedance modulus is characteristic of both the imaginary and real parts. However, for most of the measurements performed in this thesis the imaginary impedance was small relative to the real impedance. For example, EIS measurements on liver samples showed that the real part of the impedance amounted to over 99% of the modulus, while the amplitude of the imaginary impedance was about 8% of the amplitude of the modulus. Therefore it is reasonable to conclude:

$$Z_{modulus} \approx Z_{real} \tag{10}$$

The imaginary part of the impedance is still useful for tissue analysis, as it is affected by inputs that the real part of the impedance is not as affected by. For example, grounding issues will later be discussed (Chapter 3.4.3 Multiplexer Ground Setup) that were particularly noticeable in the imaginary impedance data but not very noticeable in the real (or modulus) impedance data. Additionally, the real and imaginary parts of the impedance give different information about the structure of the tissue. The real part of the impedance is the purely resistive portion of the tissue. Although exact cellular representation is complex, it can be said that the real portion of the impedance arises from the intercellular region, while the imaginary portion of the impedance (capacitance) arises from the interactions between membranes of different cells (Dean et al., 2007). Both the magnitude and sign of the phase shift relates to the electrical properties of the tissue. Negative phase shifts mean that the tissue is displaying a capacitive electrical response, while positive phase shifts mean that the tissue is behaving as an inductor. The larger the magnitude of the phase shift, the more pronounced the capacitive or inductive response of the tissue.

As was previously mentioned, the measurements were executed in the four electrode configuration: two electrodes injected current and two measured voltage (Figure 1). For imaging purposes, it is important to assign a physical location to this four electrode measurement i.e. a reference location. While, the current flows through a three-dimensional tissue volume, only a discrete impedance value can be measured (Figure 1). For simplification, the discrete impedance values are assigned to the center of the four electrode measurement: all data and contour images that are reported follow this simplification.

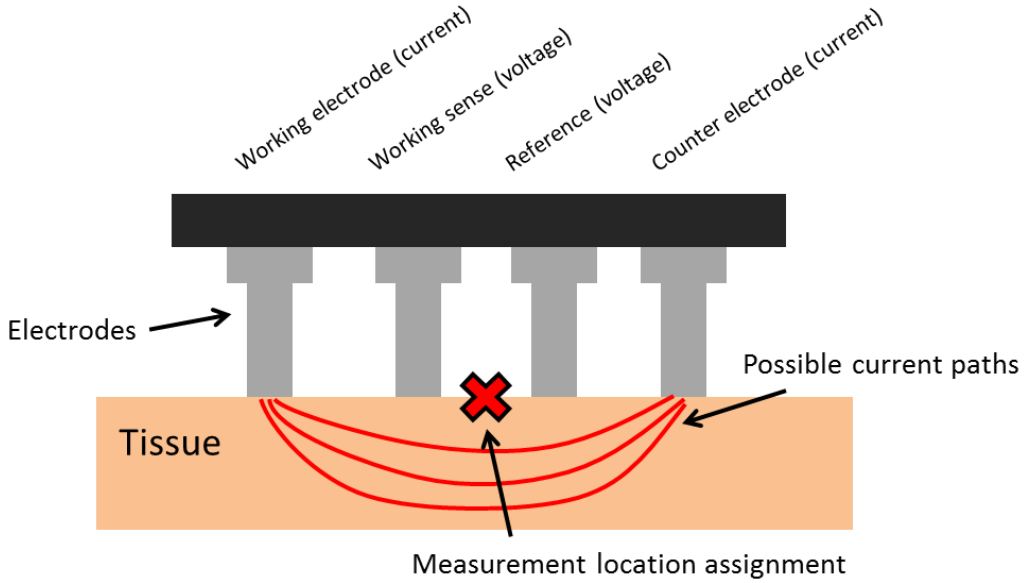

Figure 1: A schematic of a single, four-electrode EIS measurement.
The measurement location that is assigned to each measurement is the center of the four electrodes.

1.3 Present Measurement Techniques and New Objectives

For single EIS measurements, a single, four-pinned (or 4-electrode) probe was used to conduct electrical measurements on tissue samples. The probe pins are made of platinum wires of diameter ~ 400 µm, sharpened by mechanical grinding to a tip size of ~ 80 µm and a pin pitch of 1.5 mm. To generate contour images of the tissue, the single probe uses a three-axis stage to physically translate the probe to different locations in the tissue. Once measurements were performed at all locations in the tissue, an image is generated by mapping discrete impedance values. Post-processing software allows for the interpolation between these discrete points, and for the generation of contour impedance maps. Multiple disconnects arise between this measurement technique and the eventual, planned implementation of the measurement device.

Since the long-term goal is the implementation of the device in a surgical environment, the device should be 1) small and portable, to fit into the hand of the surgeon and to be easily manipulated and managed, 2) automated and rapid, to give real-time feedback to the surgeon (on the order of a few minutes at most), and 3) capable of defining a quantitatively precise and accurate surgical margin.

While the four-pinned probe is small enough to fit into the hand of the surgeon, the three-axis stage is much too large (it occupies a table-top space approaching a cubic meter, see Figure 2).

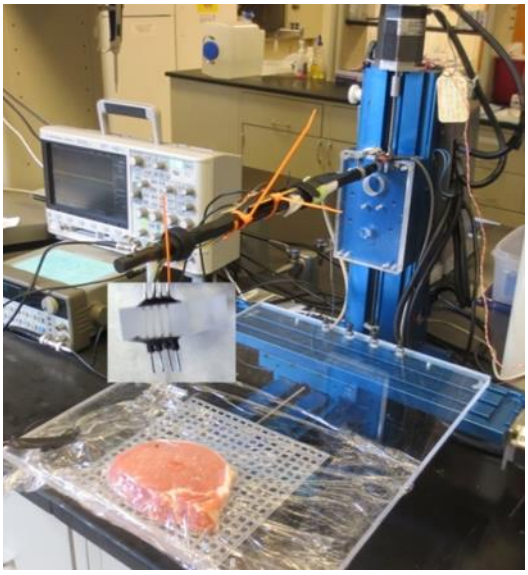

Figure 2: Three-axis stage in current use by the Prakash group.
The stage can be attached with the single-measurement EIS probe or an eddy-current probe (also used to measure tissue conductivity). The single-measurement EIS probe is pictured here.

Not only is the stage too large for clinical implementation, it is also much too slow. Previous work shows that contour images made from 25-30 discrete points (Figure 3) can take well over an hour to generate. In this regard, the current measurement system also fails in its potential to be implemented as a surgical tool. To be able to verify his/her visual and/or sensed surgical margin, the surgeon must be provided with a near real-time image (impedance map) of the region of the tissue being probed.

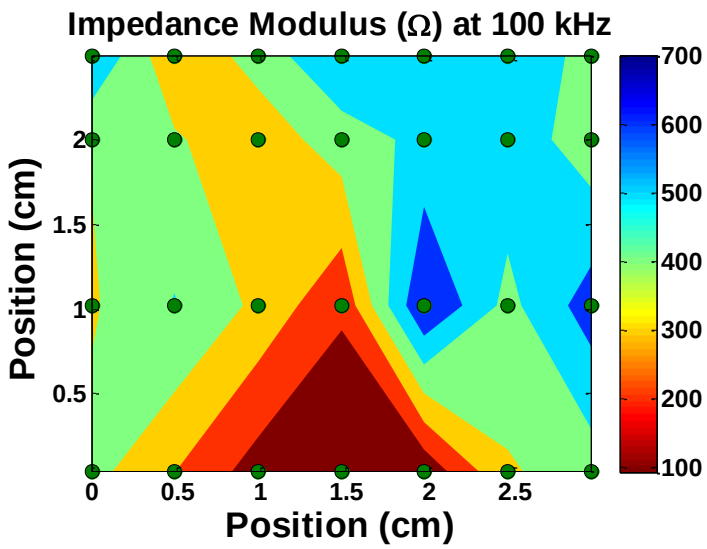

Figure 3: A contour image of a tissue surface, produced by mapping impedance values. Figure provided by Karen Bellman & Emily Sequin, and was produced through manual translation of the single EIS probe. The dark red region is the location of a tumor. If measurement resolution was increased, the tumor would appear as a circle rather than a triangle.

Measurement resolution is the last major problem with the current single-probed measurement system. Currently, measurements are taken 5 mm apart from one-another. This spacing is limited by the precision of the stage's movement, as well as the pin pitch of the single probe. Additionally, physical movement introduces the uncertainty that the probe may measure locations that have already been probed: an uncertainty that could be eliminated if the device was stationary.

The new design, explained in this thesis, will eliminate the use of a single probe and translating stage with a pin array and multiplexer, referred to as the microarray probe. The main contribution of this honors thesis is in the concept of a non-translational technique of collecting impedance data over the surface of a tissue with a local reference for each point. The design will prove to be: 1) smaller, requiring no large three-axis stage for measurements at varying locations 2) quick, completing measurements in 1-2 minutes instead of 30-90 minutes and 3) of a finer

spatial resolution, shrinking the distance between measurements from 5 mm to 1.27 mm. As a first generation prototype for testing and engineering implementation for proof-of-concept testing, all of these improvements will be accomplished using inexpensive and easily-acquired materials from commercial vendors. The total cost of the multiplexing portion of the tool is less than $150, in comparison to industrial multiplexers that can cost upwards of $3700 (as compared to Agilent Technologies E8460A reed relay multiplexer).

1.4 An Overview of the Thesis

The following two chapters will discuss the design and construction of the first and second device prototypes. The first prototype (Chapter 2) was an experiment aimed at determining if electronic switching could successfully eliminate the need for physical translation. The second prototype (Chapter 3) would improve many aspects of the first prototype, most notably increasing the number of automated measurements from 4 to 26, allowing the generation of a contour impedance map: an image of the tissue's surface. Remaining chapters will be focused on measurements performed on excised human hepatic tissue (Chapter 4). A discussion (Chapter 5) will be presented that analyzes the prototype's improvements over the tool in current use by the group, and future work will be outlined that should be performed before implementation of the tool into the hands of a surgeon.

CHAPTER 2. FIRST PROTOTYPE

The first prototype was aimed at accomplishing two goals. The first goal was to show that a pin array coupled with switching electronics can sample tissue impedance across an area and replace the need to physically translate a single-measurement probe. While other multiple-measurement EIS setups may use a combination of stationary and floating electrodes to measure impedance in different locations, all of the electrodes in the device to be described are floating. That is, each measurement is independent from past/future measurements in other locations, as each measurement uses a unique set of input/output pins. This feature is described in more detail in Chapter 5.2 Microarray Probe Comparison to Patent, when the completed microarray probe (second prototype) is compared to a previous method of multiplexing electrical impedance measurements.

The second goal was to show that a pin array has the ability to differentiate between varying tissue types, similar to the single probe i.e. there is no difference in the end-result of the tissue type classification. The first prototype was limited to the testing of bovine and porcine tissues (Figure 4) as phantoms to human healthy and cancerous tissues.

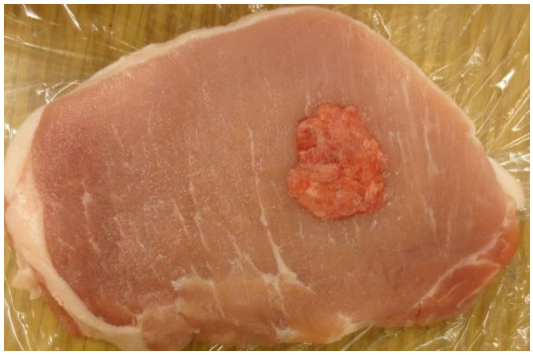

Figure 4: Bovine (dark red) and porcine phantom tissues.

The pin grid array (PGA) (Figure 5) used in the first prototype was bought as an off-the-shelf electronics component, and will be discussed in further detail in Chapter 2.2 Detailed Description of System Components.

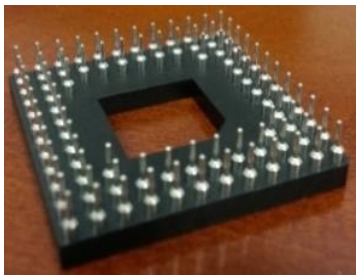

Figure 5: Photograph of the first prototype pin grid array (PGA).
The PGA was used to replace physical translation of probe with electronic switching of pins.

2.1 Switching Logic

The fundamental method used for the non-translation, multiple-location impedance measurement technique is multiplexing. Multiplexing involves connecting one channel (either input or output) to multiple channels (either output or input). A simple example of multiplexing is seen in all modern televisions, which have the ability to switch to one out of many different channels, given the user chooses a specific channel at a specific time-instance. The inputs from the potentiostat (Gamry Reference 600) were multiplexed to the pin array, so that multiple pins on the pin array have the ability to connect to each potentiostat input, but so that electronic switches can control which path to activate for a particular measurement.

To understand the difficulty behind the construction of such a multiplexer, it is important to remind the reader that the EIS potentiostat requires four pins to perform just one measurement. Two outputs (working and counter electrodes) from the potentiostat input an alternating current into the sample being measured, while two other inputs (working sense and reference) to the potentiostat record an alternating voltage response (Figure 6).

Figure 6: Gamry Reference 600 Potentiostat with two inputs and two outputs.
Green (working electrode), blue (working sense), white (reference), and red (counter electrode).

Since the EIS measurement itself requires four electrodes, the multiplexer needed to have the ability to multiplex four different channels (two input, two output) into each pin on the pin array. Note that the second prototype (Chapter 3) has the ability to connect any pin on the pin array to any of the four connections to the potentiostat. However, the first prototype was simplified in such a way that each pin on the pin array was assigned to a specific connection on the potentiostat. Electromechanical relays were used to break or bridge the connections between potentiostat and pin array, and the relays were controlled through the use of a microcontroller (Figure 7).

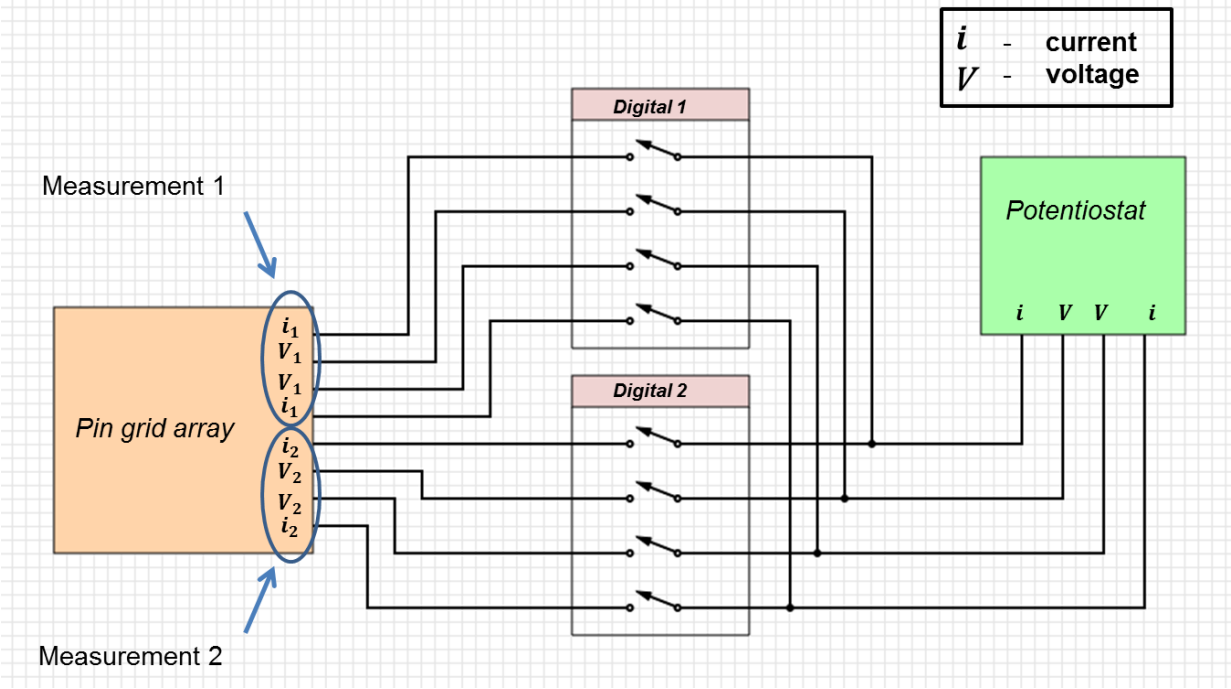

Figure 7: Schematic of the multiplexing of the potentiostat to the pin grid array (PGA). Figure shows the simplified case of only 8 pins on the PGA, leading to two possible EIS measurements. Digital 1 & 2 represent groups that are turned on/off (by signals from a microcontroller) at differing times. The arrows inside of the digital groups represent relays which are used to either break or bridge the connection between the potentiostat and pin grid array.

Since the goal of the first prototype was to test the switching mechanisms as well as the ability of the probe to differentiate between tissue types using impedance data, it was deemed not necessary for the prototype to be able to produce a complete, contour impedance map of the tissue samples (refer back to Figure 3 for a coarse example). Therefore, the first prototype was constructed so that only four EIS measurements—requiring 16 pins on the pin grid array—could be performed.

2.2 Detailed Description of System Components

There are three major components that make up the first prototype: an Arduino Mega microcontroller; a circuit made up of an array of electromechanical relays; and a pin grid array manufactured by Mill-Max (see Figure 8,Figure 9, and Figure 10).

A total of 16 reed relays (Figure 8) were required for the multiplexer setup, one for each pin in use on the PGA. Reed relays were chosen because of their low contact resistance. It was desired to minimize the contact resistance of the relay because the measured impedance value of the sample is the sum of the sample's impedance plus the resistance of the measurement system. The reed relays used in the first prototype, the Coto Technology 9007 relay, have a contact resistance of 0.2 Ω. As will be seen in the results, the impedance of the porcine tissue was measured to be about 60 to 70 Ohms, so error caused by the reed relay's contact resistance should have been less than one percent. However, since the first prototype was used exclusively to serve as a first-test for the multiplexing mechanism, not enough data was collected to check the validity in assuming contact resistance of the relays was negligible to the overall measurement.

The relays allowed for the passage of EIS signals (analog signals) depending on the state of the relay, which was controlled by the Arduino Mega microcontroller. To allow for the passage of a signal through the relay, a 5 V digital signal was sent to the coil of the relay, which was by default closed. This operation allowed for easy multiplexing of the EIS signals after construction of the circuit was completed; however, construction of even just the four-measurement multiplexer was tedious as an independent relay was required for every measurement pin, and four wires were necessary to control and use each relay: two for control of the relay from the Arduino and two for the signal that would be either passed or not passed depending on the state of the relay. The large amount of components required to multiplex just four measurements was noted as a characteristic that should be improved in the second prototype.

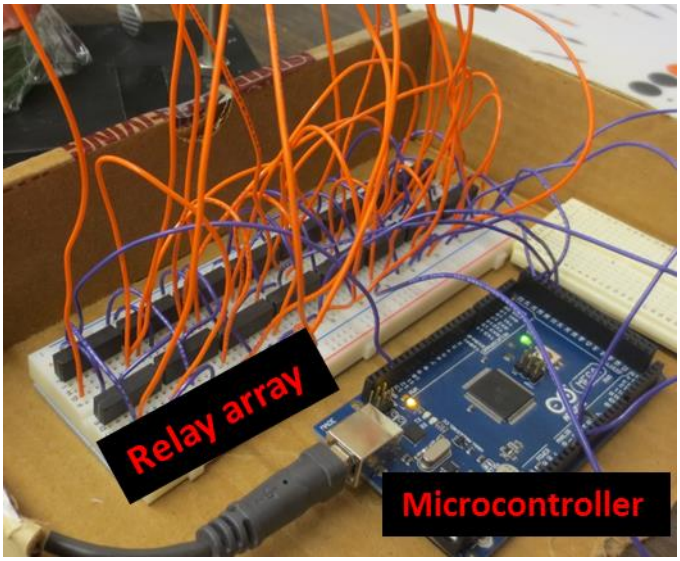

Figure 8: Reed relay array (8 by 2) seen next to the microcontroller.
64 wires (4 for each relay) were required for the multiplexing of only four EIS measurements.

The first prototype probe was built from a Mill-Max, 84-pin PGA (pin grid array) with a 2.54 mm pin pitch, as seen in the following arrangement:

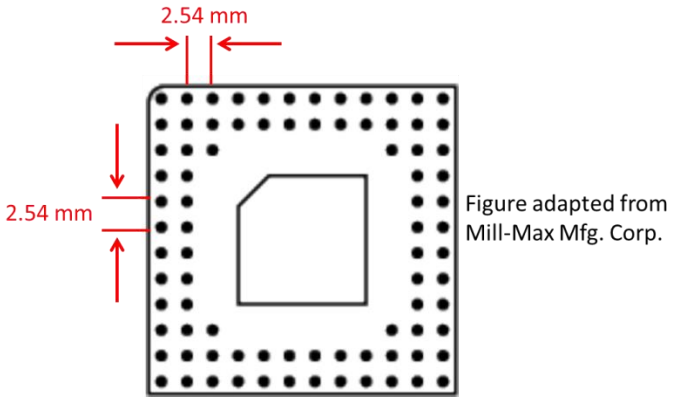

Figure 9: Layout of the PGA used as EIS probe in first prototype.

The pin grid array was noted to be non-ideal for the multiplexing of more than four EIS measurements because of its large gap in the center which would prevent the generation of a complete impedance map across the face of a tissue sample. However, the array was deemed acceptable for the first prototype because it was easily obtained as an off-the-shelf part. A

complete pin array, with no gap in its center, would later be implemented in the second prototype, when enough measurements were taken to generate a spatial impedance map.

One of the strengths of the multiplexer setup is that it did not significantly change the experimental procedure as compared to running a single EIS measurement. Once the probe was placed in contact with the sample, the single EIS measurement was set to run a loop of four measurements using the potentiostat's software, with a short time delay in-between each measurement. The Arduino software, which controlled which relays to turn on or off, was synchronized with the same time delay (5 seconds). This meant that the active measurement pins on the PGA were changed while the potentiostat was waiting in-between measurements.

While the time delay method of switching pins was successful when multiplexing only four EIS measurements, this was noted to be a weakness of the system because the microcontroller and potentiostat could potentially become unsynchronized when adding more measurements to the experiment. Actual digital communication between the potentiostat and microcontroller was a feature that would be implemented in the second prototype.

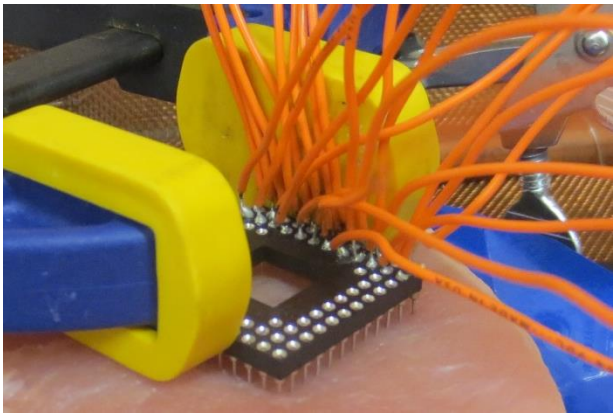

Figure 10: Pin grid array in position to measure a porcine tissue sample.

2.3 First Prototype Results

While the first prototype would eventually be used to test electronic pin-switching as well as the probe's ability to differentiate between tissue types by analysis of impedance values, two other significant experiments were first ran to explore the effect of altering injection current and altering the size of the tissue sample.

2.3.1 Varying Injection Current

The RMS value of the alternating current the potentiostat inputs through the sample is normally set to 30 μA. This value was decided upon based on previous EIS literature, but it was deemed valuable to explore if changing this current would produce the same impedance values in tissue samples. The hope was to eliminate injection current as a variable that would change the EIS response of tissue samples. Measurements were conducted using only four pins of the first prototype PGA (multiplexing was not active during this experiment) while varying the injection current. The following EIS data was collected on a porcine tissue sample.

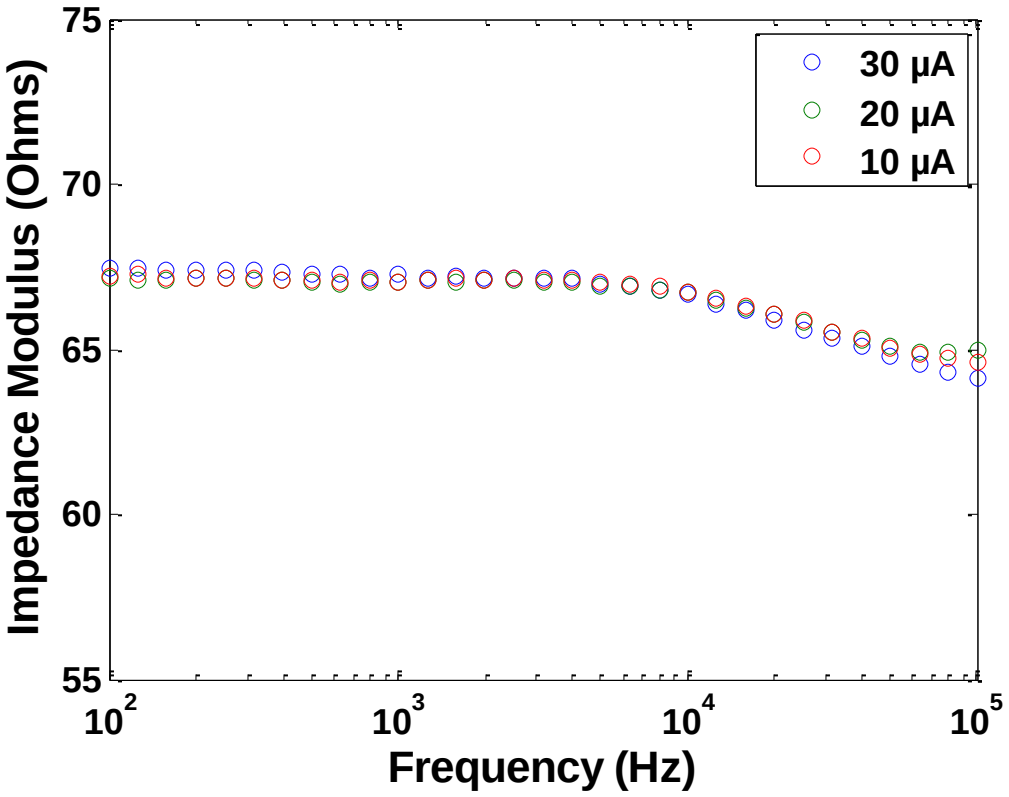

Figure 11: The effect of decreasing injection current in 10 µA increments.
Porcine muscle tissue sample.

Additionally, EIS data was collected on the same porcine tissue sample, but the injection current was decreased by orders of magnitude. The results are seen in Figure 12.

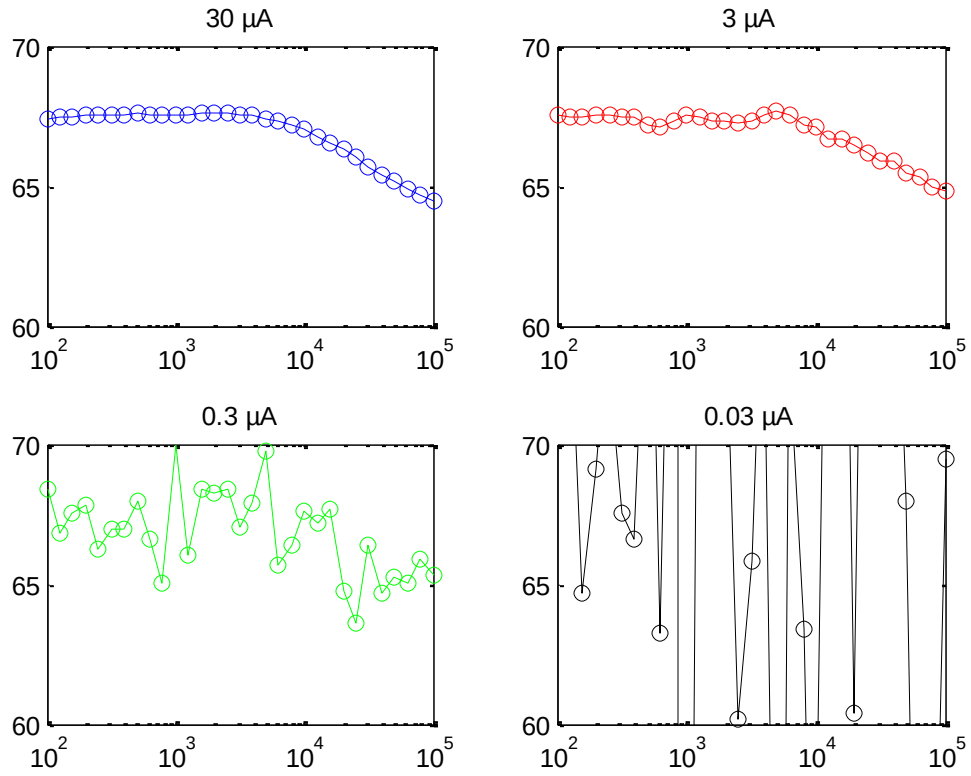

Figure 12: The effect of decreasing injection current by orders of magnitude.
Axis labels were omitted to decrease clutter. For all plots, the y-axis is impedance modulus, in Ω, and the x-axis is frequency, in Hz.

The data from Figure 11 and Figure 12 show that the injection current can indeed affect the measured impedance values of tissue samples if the current goes below a certain threshold. For data collected in Figure 11 and Figure 12, all variables except injection current (including the particular porcine sample) were kept constant. From Figure 11 and Figure 12, the minimum acceptable threshold appears to occur at about one order of magnitude smaller than the standard 30 µA. In that range, the response of the tissue sample begins to become small enough to be significant affected by the noise of the measurement system. From Figure 11, however, it can be concluded that varying the injection current from 30 µA to, for example, 20 µA does not significantly affect the measured impedance values. As 30 µA is above the observed noise threshold, this injection current is confirmed as acceptable for use in this system.

2.3.2 Varying Thickness of Tissue Samples

It was known that the size of the porcine and bovine tissue samples would vary, so an investigation into the effects of sample thickness on measured impedance was completed (Figure 13).

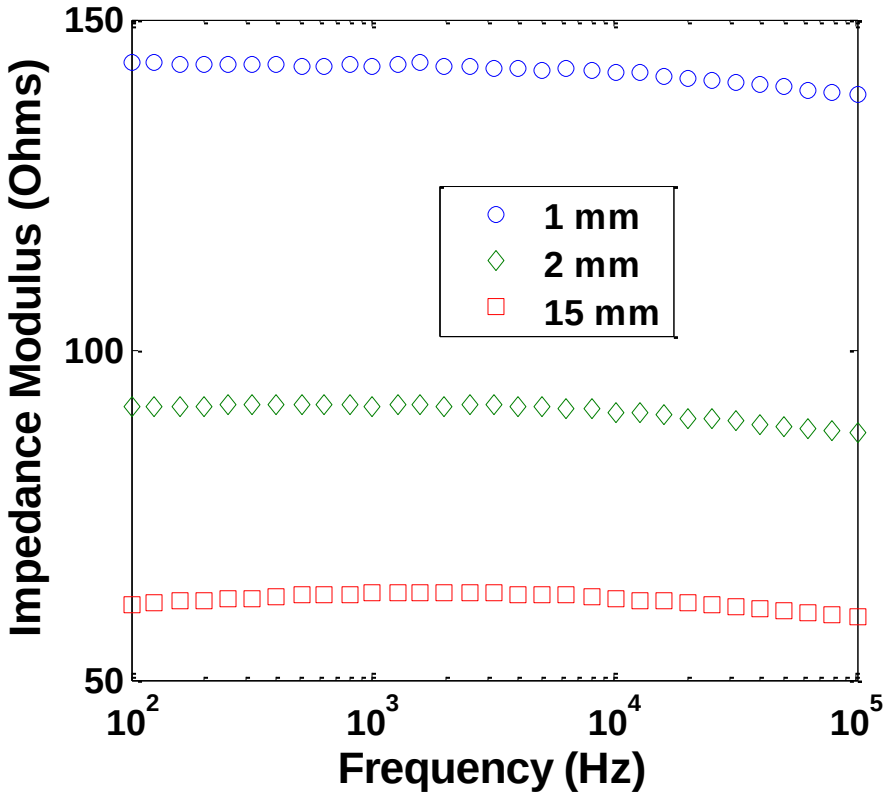

Figure 13: The effect of sample thickness on the impedance of porcine tissue. Impedance is inversely proportional to sample thickness.

The fact that the measured impedance of a sample will change due to thickness should not compromise the effectiveness of the multiplexed EIS measurements, as long as sample thickness is kept relatively uniform. Additionally, the thickness experiments do give information on why impedance values may differ from sample to sample (e.g. in samples of same composition but differing thickness) and also highlights the importance of obtaining samples that are uniform in thickness. That is, it is ideal for any specific tissue sample to be the same thickness at both the

tumor and non-tumor locations so that differences in impedance may be attributed to differences in composition and not differences in thickness.

2.3.3 Phantom Measurements

With the conclusions from the injection current and sample size experiments, the multiplexer and pin grid array probe were ready to be tested on bovine and porcine phantoms. To achieve similar sample thickness for both types of tissue, a portion of the porcine tissue was removed and replaced with bovine tissue. The sample tested was of the thicker variant, at about 15 mm, and is shown below.

Figure 14: Photograph of the porcine/bovine phantom.
The dark red tissue is the bovine phantom, representing a tumor.
The porcine phantom represents normal human tissue.

Of the four available measurement positions, two were placed in the bovine tissue and two were placed in the porcine tissue. With a pin pitch of 2.54 mm (0.1”), it was possible to confirm by sight that all four pins of a single measurement were in the correct tissue. The potentiostat was set to run four iterations of a galvanostatic EIS measurement at 30 µA, with a delay in-between measurements to allow time for the microcontroller to switch active pins on the pin grid array,

thus changing the measured sample between bovine and porcine tissue without physical translation of the probe. Figure 15 shows the EIS results of the porcine/bovine phantom sample.

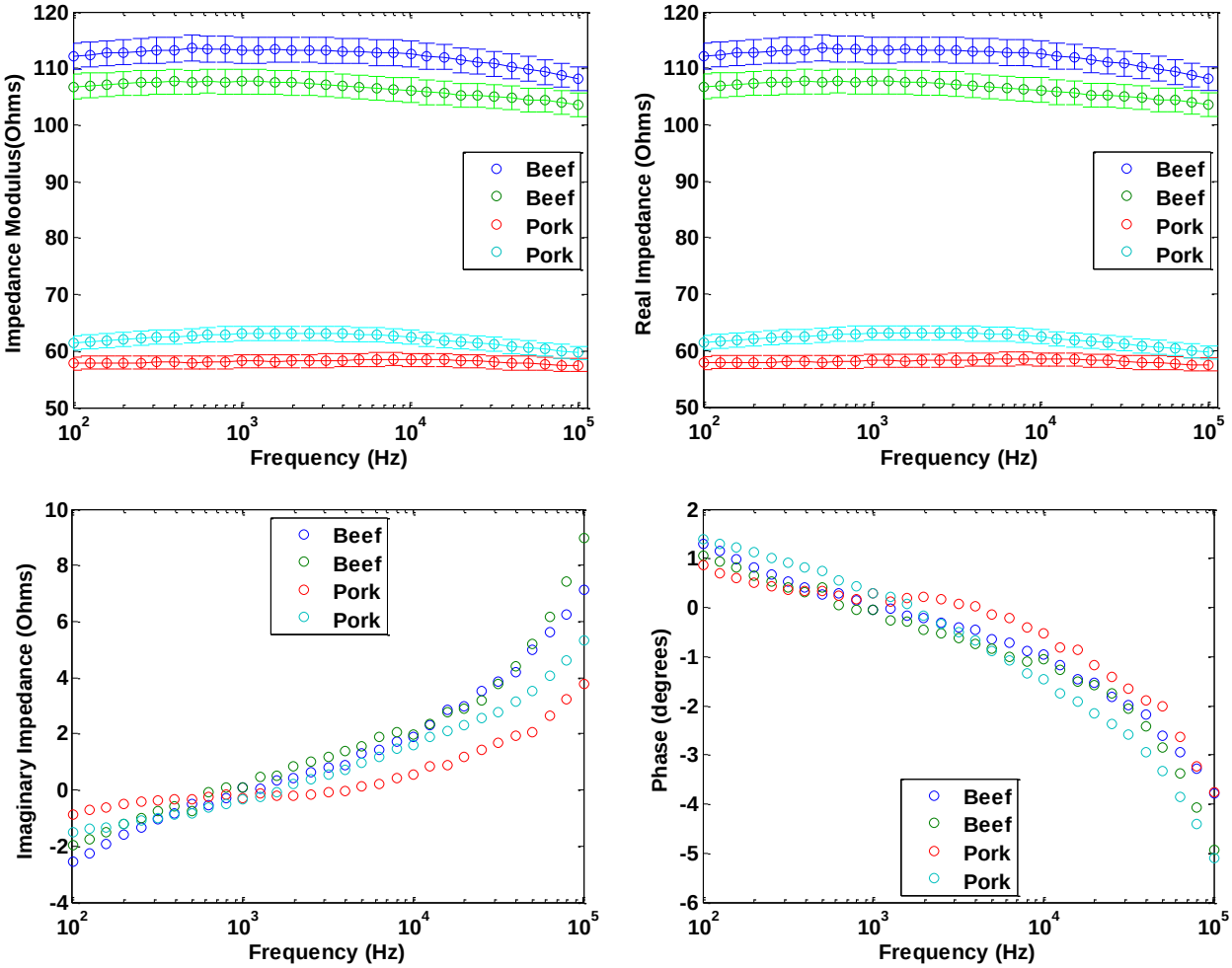

Figure 15: First prototype EIS data of porcine and bovine phantoms.
Error bars (top-left and top-right) are a 2% uncertainty window (1% for potentiostat variability, 1% for reed relay resistance). Error bars for imaginary impedance data and phase data are not provided as they are smaller than the data markers.

The above figure shows the real, imaginary, and modulus impedance values over the frequency range of 100 Hz to 100 kHz. The impedance modulus is the magnitude of the real and imaginary portions (equation 9).

The imaginary portion of the impedance for the porcine and bovine tissues was small across the frequency range (hovering between -3 and 4 Ω from 100 Hz to about 30 kHz), which caused the

real and modulus impedance values to closely match (the average difference was less than 50 mΩ). Both real and modulus impedance graphs show a bovine impedance of about 110 Ohms and a porcine impedance of about half as much at just 60 Ω (however, these values are hypothesized to be dependent upon sample thickness and thus are not valid sample-to-sample estimates of bovine/porcine impedance). From this it can be concluded that both real and modulus impedance EIS data can be used to distinguish between porcine and bovine tissue using a multiplexed pin grid array probe. Although phase and imaginary data did not show strong differences between phantom tissue types, these data types will prove valuable for differentiating between tumor/non-tumor human liver tissue (Chapter 4. Ex-vivo Human Liver Measurements).

CHAPTER 3. SECOND PROTOTYPE

While the first prototype could detect differences in tissue composition, the second prototype would be able to generate a contour image to display EIS data over an area. The overarching goal was to make a measurement probe that showcased significant improvement (versus translational techniques) in its ability to be eventually implemented in a clinical setting. To accomplish this overarching goal, individual electromechanical relays were eliminated as a possible switching mechanism, as the number of relays required to perform enough measurements to generate an image would occupy too large of a space and would require excessive connections. For example, 16 reed relays and 64 wire connections were required for the multiplexing of just four EIS measurements. If the same design was used to multiplex 26 EIS measurements, 104 reed relays and 416 wire connections would have been required. This would have made the setup occupy the space of 7 standard breadboards.

Therefore, the second prototype would replace the relay circuit of the first prototype with a series of manufactured multiplexer integrated circuits, configured specifically for EIS measurements. Additionally, the probe head was replaced so that more measurements could be taken in a smaller area (the number of active pins was increased, and the pin pitch was decreased). The goal being a final prototype that can rapidly quantify the tissue state through use of an image containing tissue structure information at the local area being probed by the surgeon. Other desired improvements were kept in mind when designing the second prototype, among them:

- Communication with the potentiostat, for synchronized measurement progression.
- A total device footprint that would be small enough to fit onto the hip of a surgeon.
- Soldered wire connections, for both durability and organization.

- Detachable probe for easy cleaning. Since the probe will be in contact with human tissue that may be infected with serious diseases, it should be able to detach from the rest of the device and be either discarded or cleaned as necessary.
- Single-pin translation instead of quad-pin translation (described further in Chapter 3.1 Logic).

3.1 Logic

To increase the number of measurements within a given set of pins, a different pin-switching logic was implemented. Instead of having every pin assigned to a specific input on the potentiostat, it was desired to have every pin be available to any of the four inputs of the potentiostat. If this could be achieved, the four-pin measurement could step a single pin at a time instead of stepping four pins at a time. It is possible to quantify the number of four-pin measurements available for an arbitrary number of pins:

Table 1: Maximum number of four-pin measurements per n number of pins per row.

Pin Step	Used in	Possible measurements per row (n pins per row)	Number of measurements in a 16 pin row (for example)
Four	First prototype	n/4 (round down to nearest integer)	4
Single	Second prototype	n-3	13

The new, single-pin step technique can drastically increase the number of available measurements per area. For example, imagine a 16x16 pin array. Using the four-pin step technique, there could be 4 measurements per row, and 16 rows of measurements, giving a total of 64 measurements; the distance between measurements would be one pin-pitch in one direction but four pin-pitches in the other. Using the single-pin step technique, there could be 13 measurements per row and 16 rows of measurements, giving 208 possible measurements; the

measurement grid produced would have equal spacing in both directions (the pin pitch). The advantage of the single-pin translation grows as the number of pins per row grows. Therefore, the single-pin step technique is an essential design requirement for pin arrays aimed at creating high-resolution images. A graphical depiction of the pin step technique can be seen below:

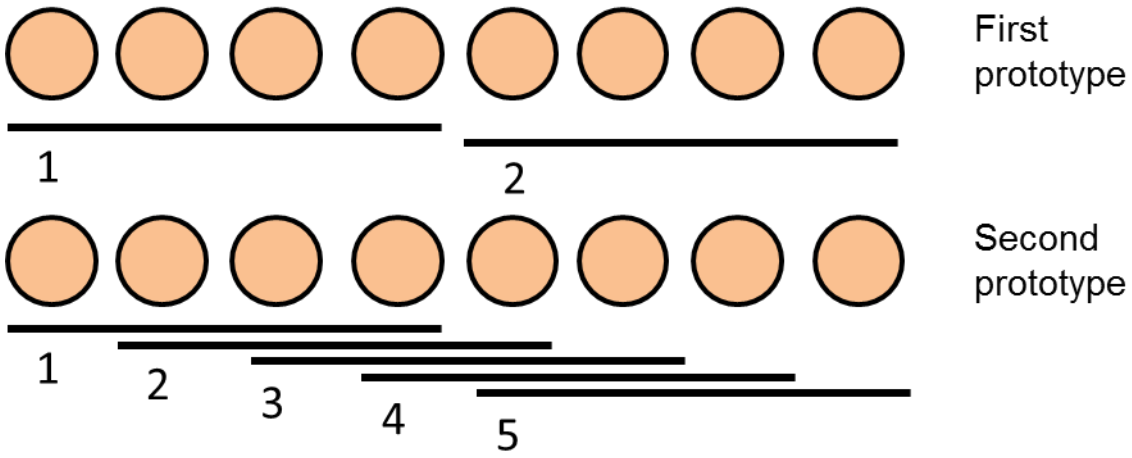

Figure 16: Comparison of the pin-switching logic between first and second prototype. Given eight measurement pins, the second prototype logic allows for five measurements, while the first prototype logic only allows for two.

Implementation of the new pin-switching logic required new switching hardware. Simple on-off relays could not efficiently make every pin on the pin array available to all four of the potentiostat inputs (for the single step logic, every pin must be able to connect to any of the four potentiostat inputs). However, a multiplexer could very easily be used to route each signal from the potentiostat to one of the pins on the pin array. Therefore, a single multiplexer was assigned to each input of the potentiostat, requiring four multiplexers in total. The maximum number of pins available to be multiplexed was limited by the multiplexer configuration: a 32x1 mux was the configuration available with the highest number of drains *or* sources (many multiplexers can operate as muxes or demuxes). Therefore, the maximum number of active pins on any chosen pin array could be 32.

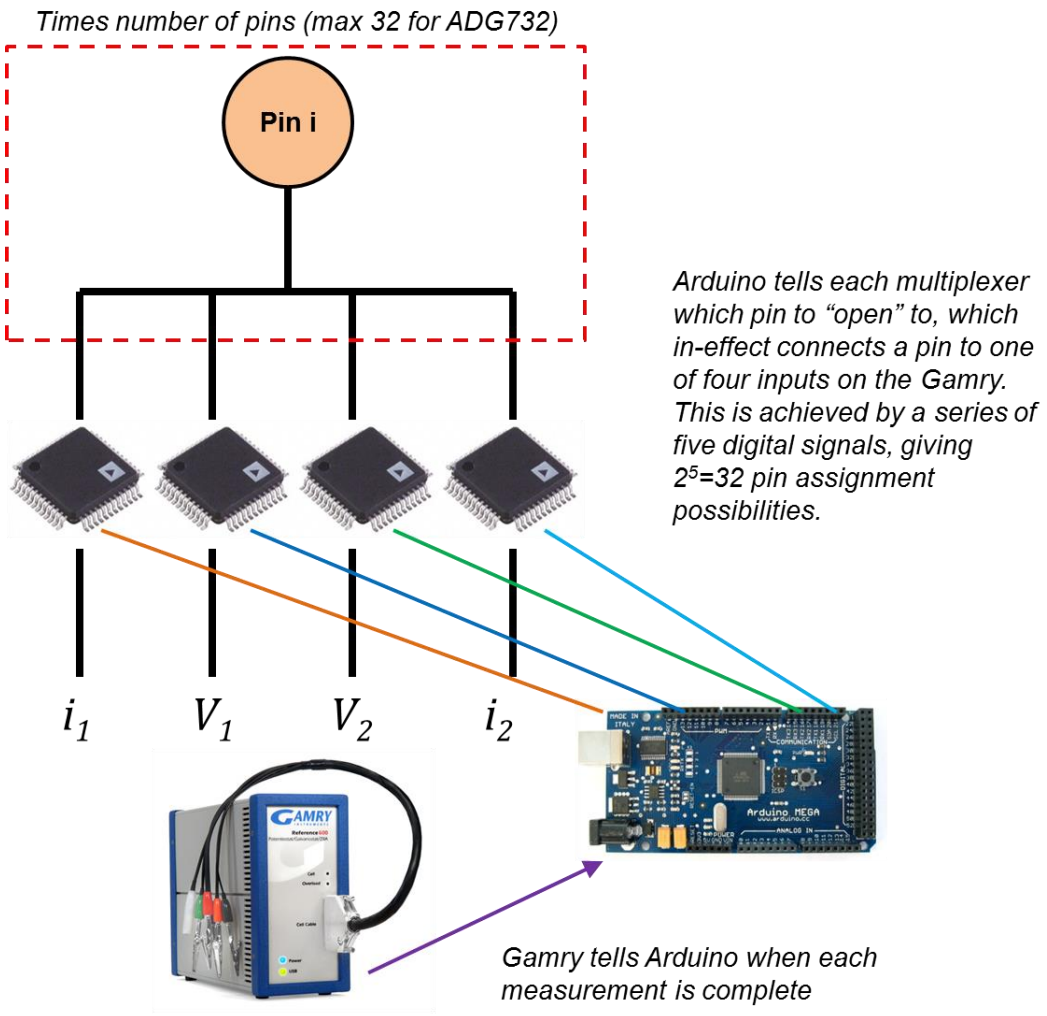

Figure 17: Schematic showing comm. between potentiostat, Arduino, and multiplexers.

Every pin in the pin array would have the ability to connect to any of the four multiplexers. However, the Arduino microcontroller was used to control each multiplexer and to tell each multiplexer which pin should currently be connected to its input. Furthermore, the potentiostat was connected to the Arduino to send a digital pulse when the previous measurement was complete, in order to tell the Arduino to switch multiplexer assignments (step a single pin). No communication from the Arduino to the potentiostat was implemented, as the Arduino operating time is less than a millisecond (16 GHz clock speed); therefore pin switching was assumed to be instantaneous. The potentiostat was set to loop its galvanostatic EIS measurement

26 times. The only inputs required by the user is to refresh the Arduino code (code feedback seen in Figure 18), and then to run the potentiostat measurement sequence (given in Appendix B.1 Second Prototype Gamry Sequence). The Arduino code was set to wait for an input (a 5 V pulse) from the potentiostat before any switching would take place. For a flowchart of measurement execution, see Figure 19.

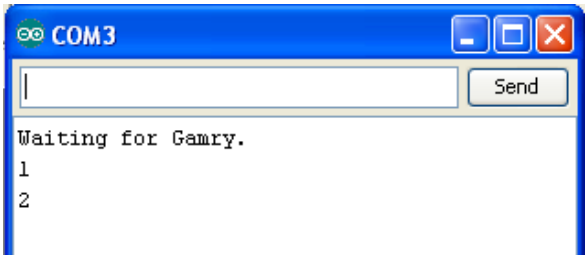

Figure 18: Arduino communication window.
Tells the user which measurement is in-progress, or if the Ardunio is waiting for the potentiostat, or if the entire EIS measurement is complete.

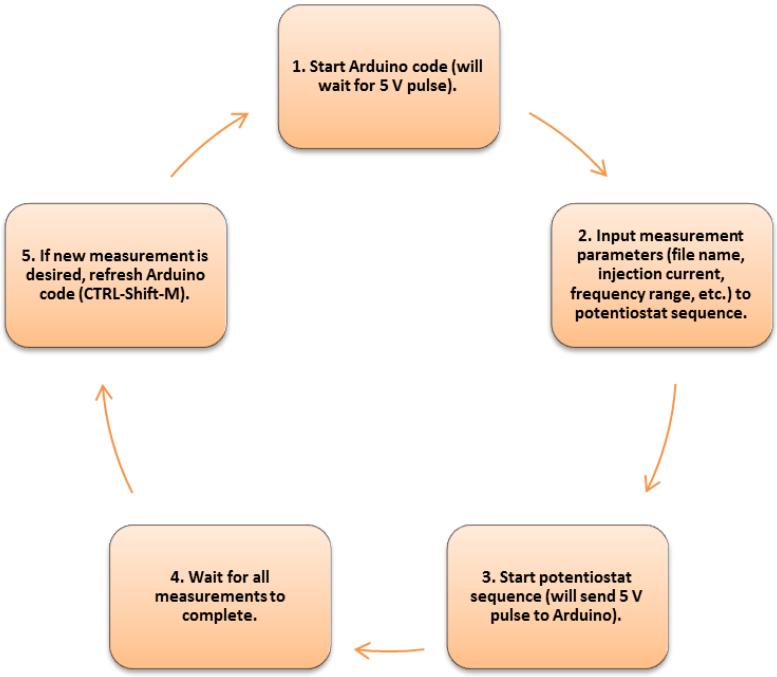

Figure 19: Second prototype measurement execution flowchart.

3.2 Construction

There were two major tasks in constructing the second prototype. The first was to make the multiplexer, which required soldering the manufactured multiplexer ICs to breakout-PCB boards, and then combining the four breakout-PCBs into a final multiplexer, which would then have four available inputs. The second task was to take the manufactured interconnect and configure it for use as a probe.

The multiplexer IC chosen was the Analog Devices AGD732, an analog 32x1 multiplexer. It can pass an analog signal from one input to any of 32 outputs. The output is chosen based on a combination of five digital logic inputs. The device was chosen because it was the multiplexer with the highest number of possible outputs available as a low-cost, integrated-circuit chip. The multiplexer has the advantage of coming in a small, 7 mm by 7 mm TQFP (thin quad flat pack) package, which allows it to be integrated to a PCB. However, this also meant that soldering the multiplexer to a PCB breakout-board would be required. To keep the cost of the total probe package low, the soldering was done by hand instead of outsourcing. With the ADG732 having a pin pitch of about 0.6 mm, soldering was a challenge, but eventually satisfactory results were obtained (Figure 20).

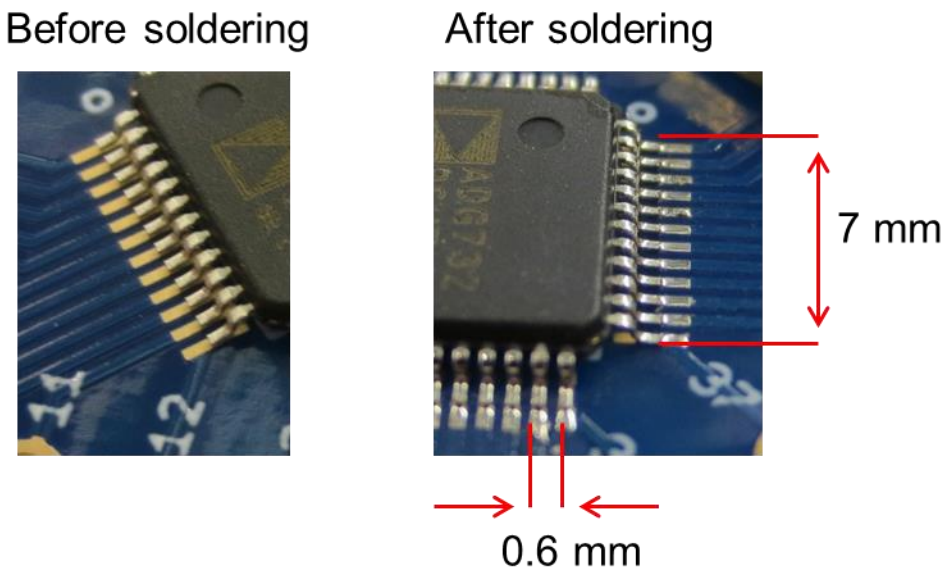

Figure 20: Second prototype multiplexer soldering quality.

After soldering the multiplexer ICs to each of four breakout PCBs, the PCBs were stacked together. This stacking design was chosen intentionally. It functioned as a low-cost alternative to custom PCB manufacturing, and enabled the finished multiplexer to avoid any wiring to create the nodes for each of the 32 pin outputs. In the future, the same connections could be made using a custom PCB and the footprint of the multiplexer could be made even smaller.

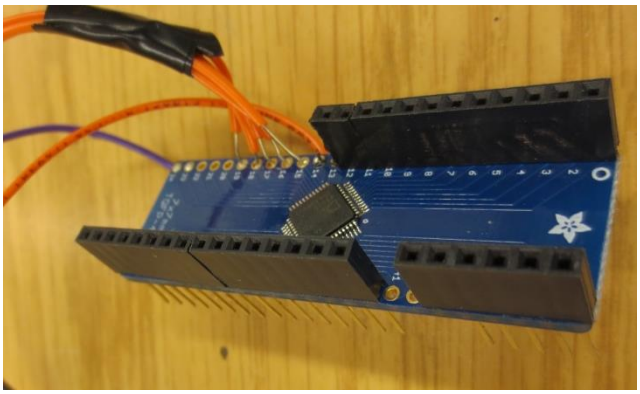

Figure 21: A single multiplexer IC soldered to a breakout board.
Four of these breakout boards stack to form the overall multiplexer. Each breakout board is responsible for one of the four inputs to the potentiostat. The stacking provided a durable method of creating the node depicted in Figure 17 without soldering.

Some additional wiring was necessary to incorporate the communication between the potentiostat and the Arduino microcontroller. A reed relay was used to send a 5 V pulse to the Arduino when the potentiostat finished a single measurement. To send a pulse, the relay's source and sink was wired to the Arduino ground and power. Then, the potentiostat's power and ground was used to turn the relay on or off (by powering the coil of the relay). After the potentiostat had completed each measurement, it would send a short pulse to the relay, allowing an Arduino input pin to sense a high signal (5 V) from its own power source. Note that the relay was necessary because the Arduino was unable to read a high (5 V) signal from the potentiostat in relation to its own (Arduino) ground.

Additionally, a small LED bulb was incorporated to flash each time the potentiostat completed a measurement, allowing for easier debugging and program progression. Once the Arduino sensed the 5 V pulse, it would switch its digital outputs (five in total) to the four multiplexers, thus switching the connections between the potentiostat and probe. Note that, while possible, communication from the Arduino to the potentiostat was not incorporated. Such communication was deemed unnecessary because the amount of time to switch digital outputs from the Arduino is less than one millisecond, while the potentiostat has a built-in delay between measurements of three seconds. See Figure 22 for a circuit diagram describing the communication between Arduino and potentiostat.

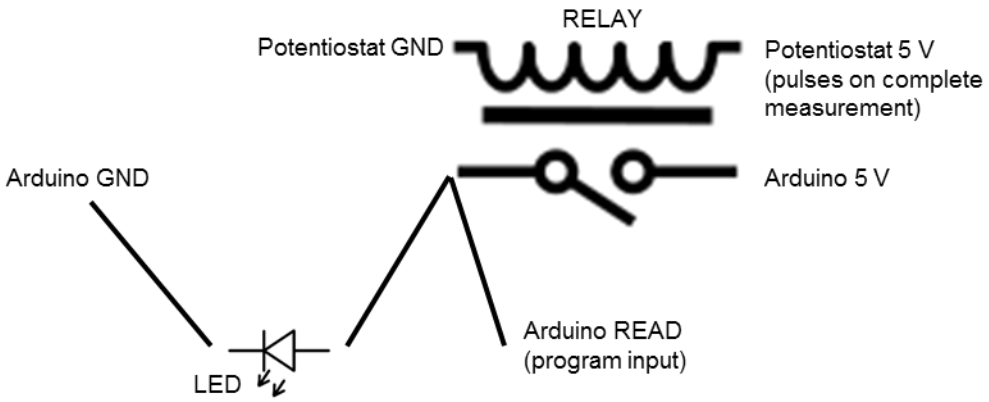

Figure 22: Second prototype communication circuit diagram.
The Arduino program input pin and LED bulb read 0 V until the potentiostat pulses 5 V, closing the relay that is connected to the Arduino 5 V.

To avoid the excessive wiring that was encountered during first prototype construction, custom wiring harnessed were built using manufactured wiring houses and snap-in wires (Figure 23). This feature, along with the multiplexer being built with almost entirely soldered or stacked (breakout boards) nodes, meant that the second prototype required about 20 wires as compared to the first prototype's 64 wires, despite increasing the number of measurements from four to 26. Figure 24 is a photograph of the second prototype, displaying the small form-factor and organization of the multiplexer.

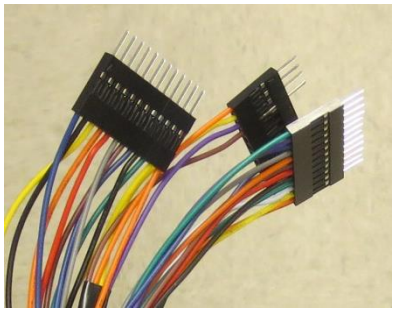

Figure 23: Custom wiring harnesses used in the second prototype.

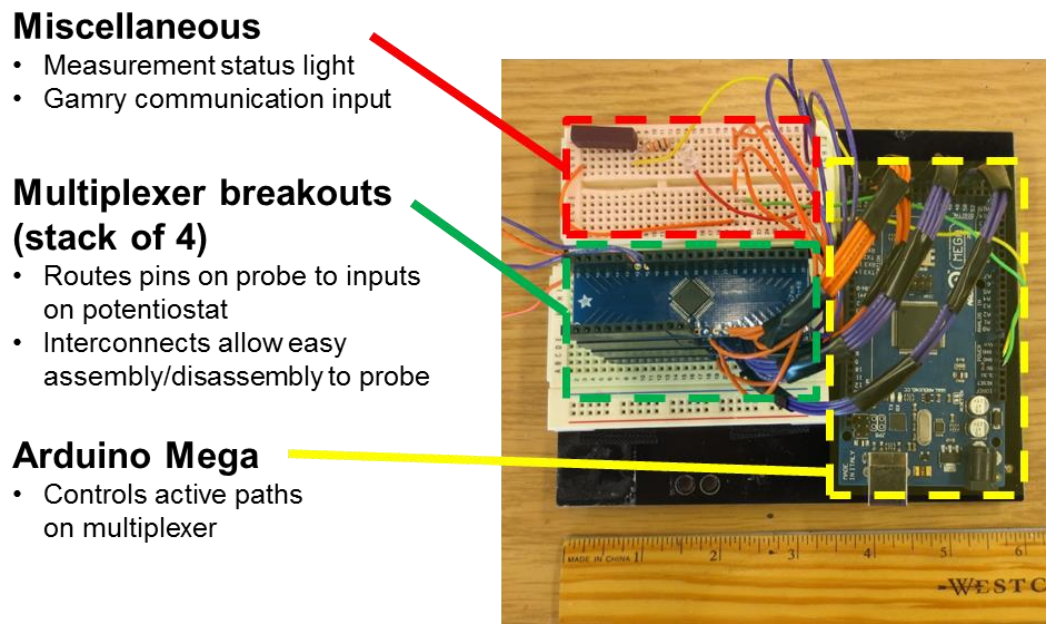

Figure 24: Second prototype in its entirety, minus the probe.
The total footprint is about 15 cm x 15 cm (6" x 6"). The relay and LED previously described are in the top-left. A picture of the detachable probe can be seen later in Figure 25.

Now that the multiplexing circuit has been described, the probe of the second prototype will be detailed.The probe was made from a Mill-Max 853-43-034-10-001000 interconnect. Critical dimensions are as follows:

Table 2: Second prototype probe specifications

Pin pitch	1.27 mm
Pin diameter	457 µm
Pin material finish	Tin
Pin bulk material	BeCu
Pin length	2.59 mm
Assembly length	20.7 mm
Assembly width	3.05 mm
Number of pins	34
Number of pins in use	32
Pin arrangement	2 x 17
Assembly insulator material	Nylon 46
Approximate cost/unit	$6.50

This interconnect was chosen with mainly three parameters in mind: pin pitch, ease of assembly (male/female), and ease of availability. Pin pitch was the foremost parameter, as it dominates measurement resolution. After exhaustive searching, an interconnect with a 1 mm pin pitch in both directions was found, manufactured by Global Connector Technology (GCT). However, GCT's interconnects at that pin pitch were only male-to-male connections. The Mill-Max probe has a less-desirable pitch of 1.27 mm, but is male-to-female, allowing easier connection to the multiplexer. Additionally, the Mill-Max probe was available for immediate shipment at a low cost (~ $6.50) from Heilind Electronics. While the chosen interconnect is easily obtainable, its rectangular (2 pins by 17 pins) shape is not ideal. A square, PGA-like platform is prefered; however, complete PGAs are rare: most come with large open slots in the center (as was seen in first prototype).

Connecting the 2.54 mm pitch (standard for through-hole electronics) wiring harness to the 1.27 mm pitch interconnect proved to be very challenging, as standard soldering could not be performed on the female wire connections in the pin array. This connection between differing pin-pitches (Figure 25, the purple wires with orange wires behind) proved to be the most fragile piece of the overall device. The electric path between final probe tip and wire harness had to be intermittingly checked. Occasionally, especially after heavy device use, a small number of the connections were observed to be incomplete; it was necessary to make time-consuming repairs to the small, fragile connection. A more rigid connection between multiplexer and pin array would be a major improvement to future iterations of the device.

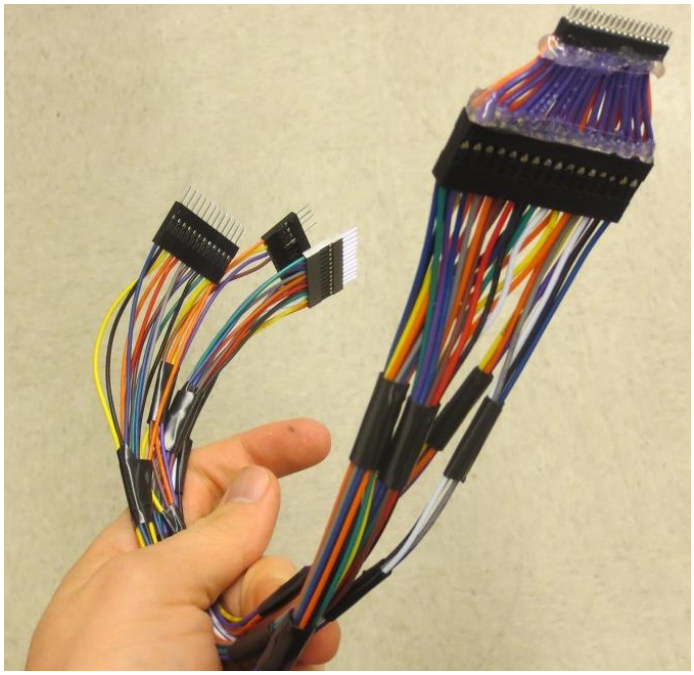

Figure 25: Second prototype probe.
The ability to be detached from the multiplexer allows for easy cleaning of the probe after experiments. Note, after contact with human tissue disinfection of the probe is also required and therefore the ability to clean the probe separately from the interface wiring to the electronics is essential. It should also be noted that any further reduction in probe size would require microfabrication and is the goal of continuing research. The purple and orange wires towards the tip of the probe are not soldered, producing fragile connections.

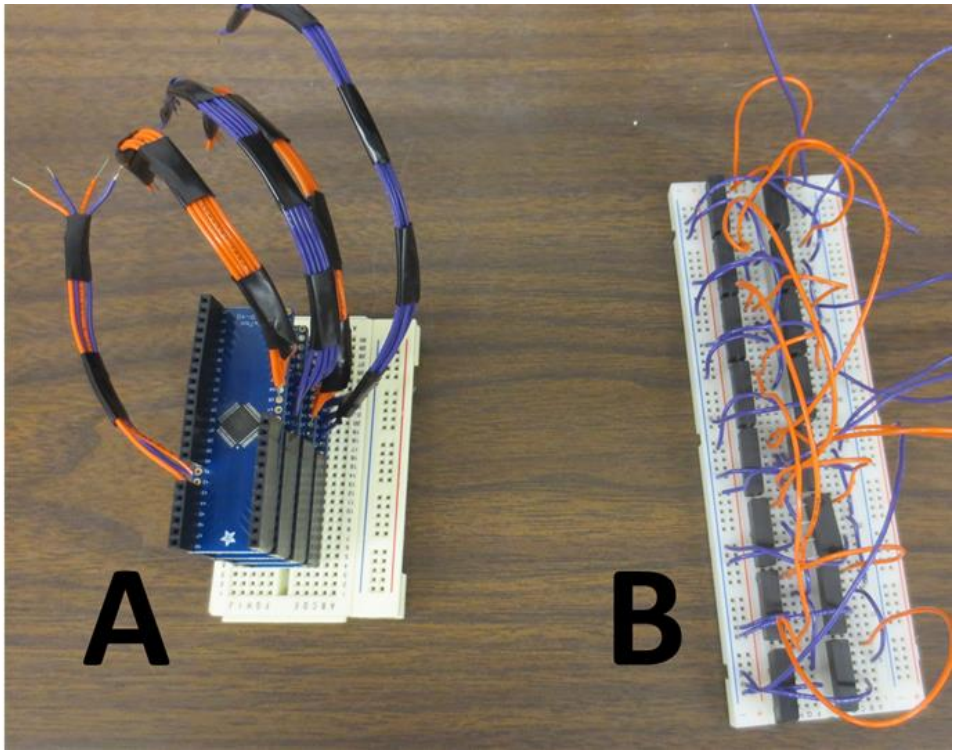

Figure 26: Comparison of prototype multiplexers.
(A) Second prototype multiplexer, capable of performing 26 EIS measurements. (B) First prototype multiplexer, capable of performing 4 EIS measurements.

While the second prototype increased the number of measurements from 4 to 26, the wiring required and the size of the switching mechanism was reduced. If looking at only the multiplexing potion of the device (Figure 26), zero loose wires are required for the second prototype setup, while 64 loose wires are required for the first prototype setup. The second prototype multiplexer occupies the area of half of a standard breadboard, while the first prototype multiplexer occupies the area of a full breadboard. The decrease in device footprint can be attributed to the multiplexer integrated circuit, which replaced 32 individual relays with a

chip less than 1 cm^2 in size. Additionally, the stacking of the four multiplexer chips drastically reduced the need for wiring and/or soldering.

Figure 27 shows a comparison of the first and second prototype probe interfaces. While the first prototype probe had a square layout (desirable for image generation) it had a large portion in the center missing pins, meaning that a full image could not be generated. The second prototype probe contained no gaps but was not square.

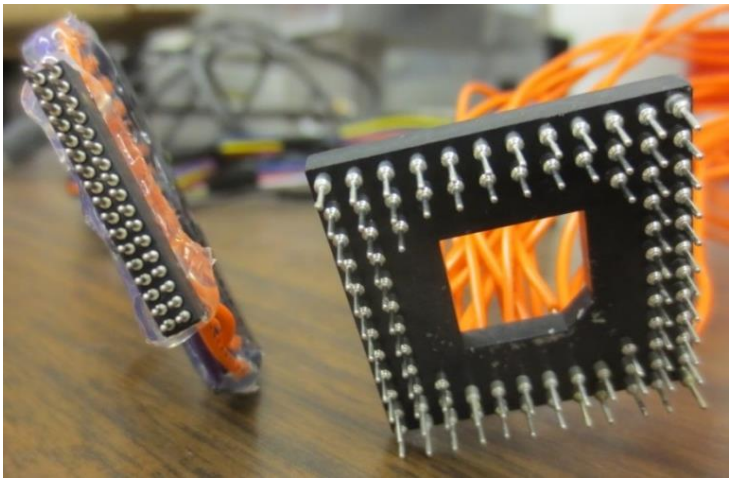

Figure 27: Comparison of prototype probes.
(Left) second prototype probe, with 1.27 mm pin pitch and roughly 2 cm length. (Right) first prototype probe, with 2.54 mm pin pitch.

3.3 Second-Prototype Measurements on Porcine Muscle/Fat

While the phantom measurements taken using the first prototype used both bovine and porcine tissue, the measurements conducted using the second prototypes were performed on porcine muscle and porcine fat. This change was made because it aligned more with the desire to eventually use the EIS tool to distinguish between tissues within the same organ but comprising distinct structural and/or chemical features, including different cellular structure.

The following figures were constructed using data from the first testing of the second prototype, and are somewhat erroneous (especially the imaginary and phase data) because of an error in

grounding that will be discussed in more detail in a later section. The region that may have been especially affected is those at high frequencies, as the impedance and phase uncharacteristically jump at the frequencies nearing 1 MHz. However, the data does display a strong ability to distinguish between tissue compositions using real or modulus impedance at intermediate frequencies (Figure 28).

Please note that EIS data taken at a particular frequency is presented as 3D bar graphs (frequency noted in figure title), while EIS data taken at all measured frequencies is displayed as line plots, with each line corresponding to measurements made at different locations within the pin array.

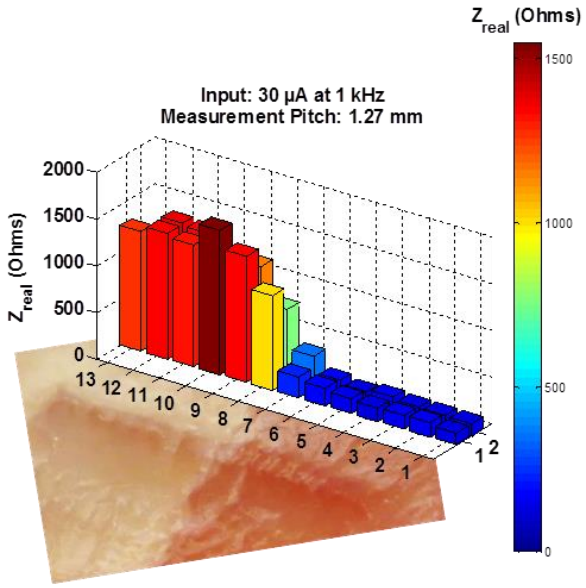

Figure 28: First image generated using the second prototype.
3D bar plot constructed from real impedance measured data measured at 1 kHz. The data is overlaid onto a digital photo of the sample: the white portion is porcine fat while the red portion is porcine muscle.

Figure 29 was taken from the same experiment as in Figure 28 but over the entire measured frequency range (100 Hz to 100 kHz) and including all three parts of the impedance (modulus, real, and imaginary) as well as phase shift.

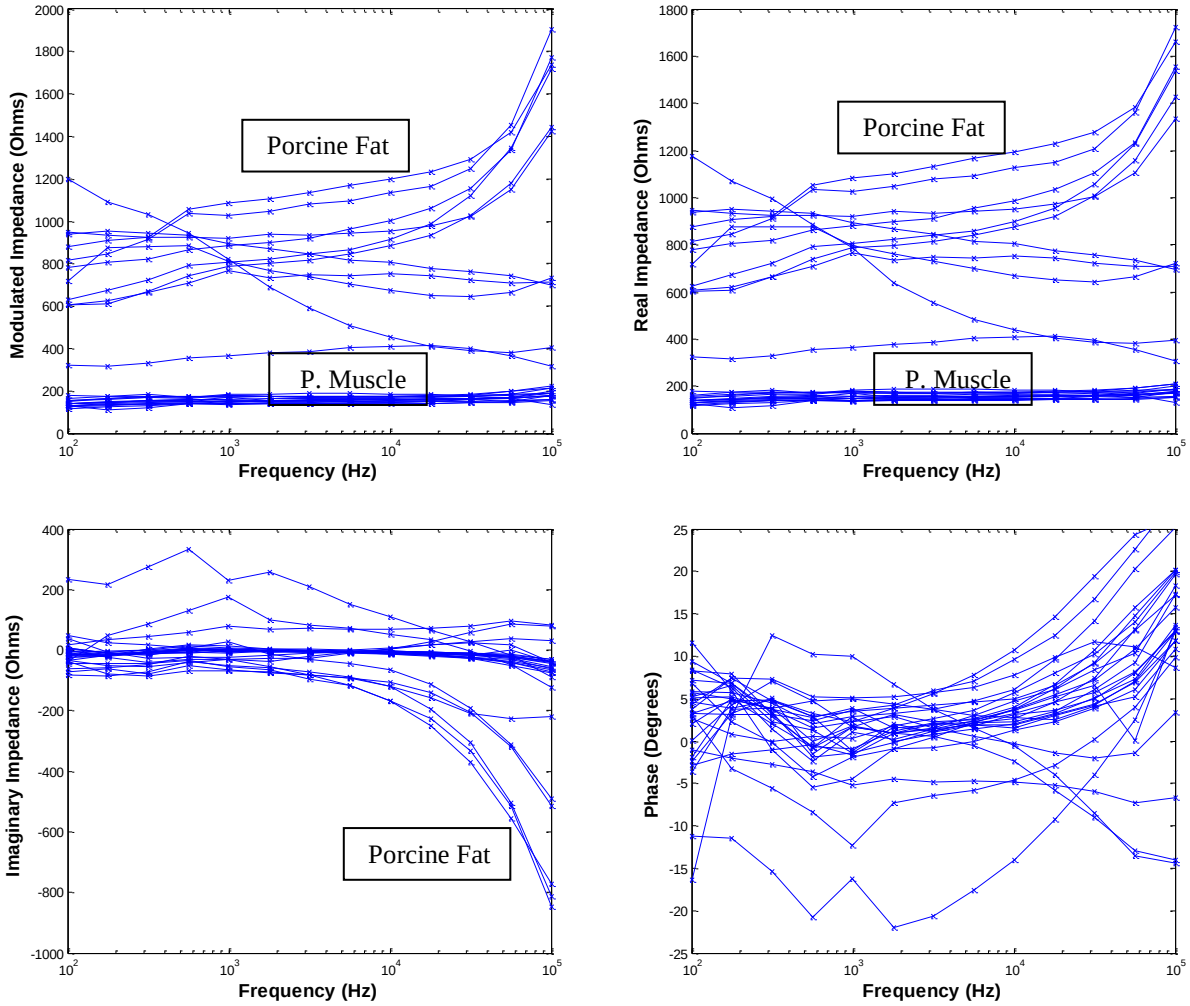

Figure 29: EIS data collected using the second prototype.
Approximately half the pins are in porcine muscle, approximately half in porcine fat. Plots labeled with tissue type show distinct patterns, while unlabeled plots imply unclear trends. Data recorded while the multiplexers were erroneously grounded.

3.4 Sources of Error and Measurement Recommendations

Initial measurements using the second prototype showed a good ability to distinguish between tissue types (Figure 28). However, it was desired to find how an EIS measurement using the second prototype probe would compare to a single measurement using the four-pin probe.

Therefore, a large effort was made to find errors that were introduced because of the multiplexer and probe. From observations made thus far, the following recommendations can be made:

- Operating frequency for accuracy: 1 kHz to 100 kHz
- Ground multiplexer to measurement device (potentiostat)
- Avoid the stacking of measurement probes

The measurements that led to these guidelines are discussed in the following sections.

3.4.1 Multiplexer Performance at High Frequency

Measurements were conducted on a dummy cell provided by Gamry Instruments in order to access the effect of introducing the multiplexer circuit between potentiostat and sample. The dummy cell is comprised of a capacitor in parallel with a resistor, followed by two more resistors in series.

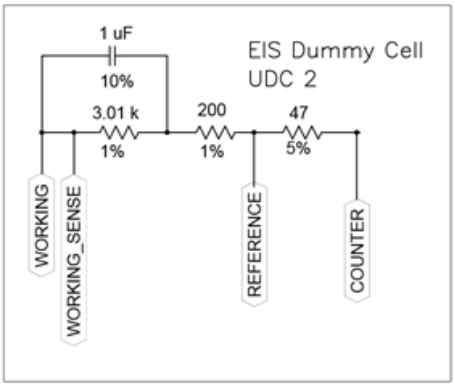

Figure 30: Dummy cell schematic.
Modified figure from Gamry Instruments Incorporated. Voltage is measured between working electrode and reference electrode.

For verification of the dummy cell measurement, the results will be calculated theoretically. The impedance of a capacitor is given below:

$$Z_{cap} = \frac{1}{j\omega c} \tag{11}$$

At high frequencies, the impedance of the capacitor approaches zero and the capacitor can be treated as a short circuit. Therefore, most of the current bypasses that 3.01 kΩ resistor and the measured impedance should be 200 Ω. At low frequencies, the impedance of the capacitor approaches infinity and the capacitor can be treated as an open circuit. The current prefers to travel through the 3.01 kΩ resistor path, followed by the 200 Ω resistor, and the measured impedance is expected to be 3210 Ω.

These results were confirmed when the dummy cell was connected directly through the potentiostat (Figure 31). The multiplexer did not introduce any significant error at low frequencies but diverged significantly from the direct connection at high frequencies (> 100 kHz). See Figure 31: between 10 kHz and 100 kHz the directly connected measurement and the through multiplexer measurement begin to diverge, especially in the phase data. The dummy cell was connected through the use of alligator clips: the probe was not used to attach to the dummy cell; therefore, the probe is not responsible for the high-frequency (> 100 kHz) deviation.

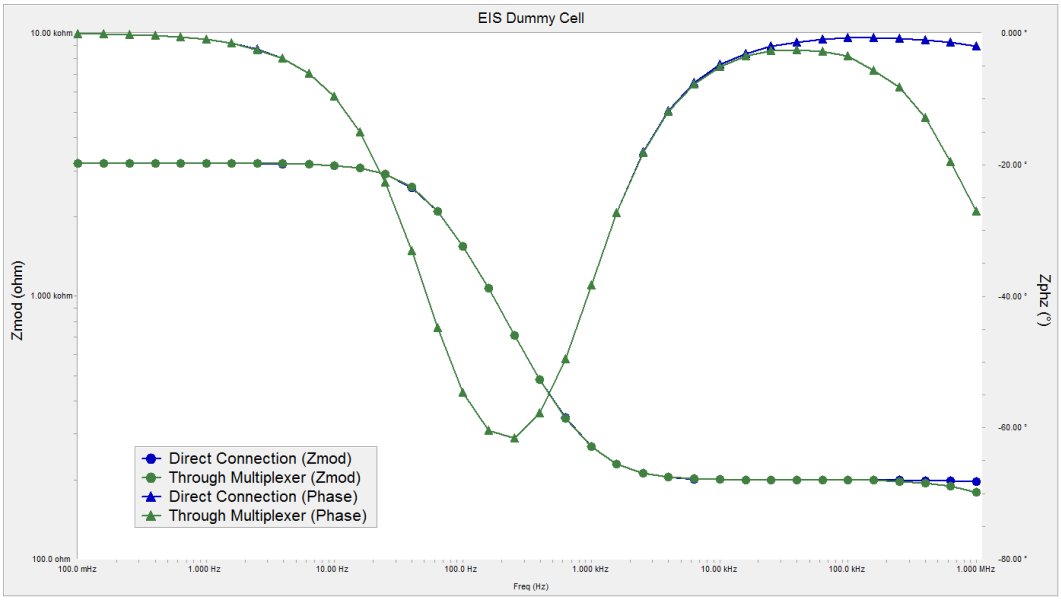

Figure 31: Impedance and phase deviation seen at high frequencies due to the multiplexer.

The dummy cell measurements showed that true EIS values may not be measurable at high (> 100 kHz) frequencies when using the multiplexer. However, high frequency data may still be useful when attempting to distinguish between tissue types. The following figure helps to illustrate:

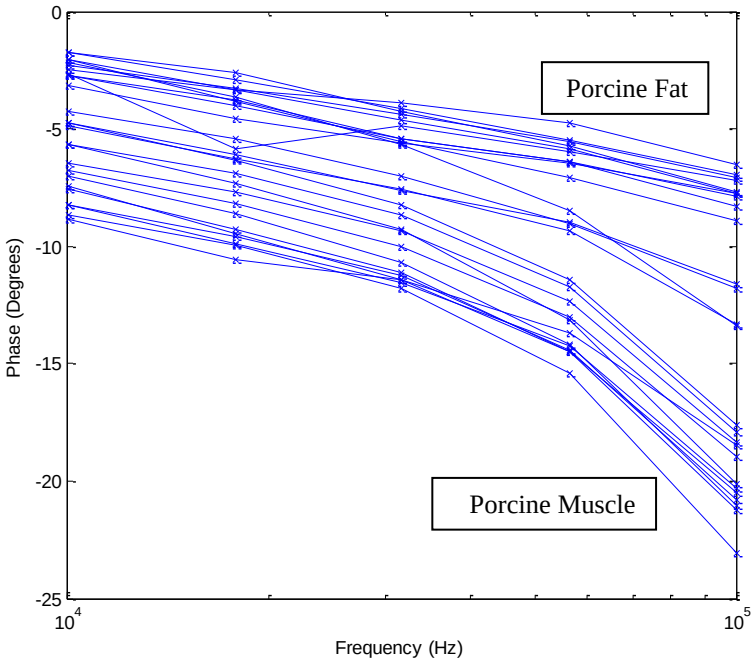

Figure 32: EIS on porcine muscle/fat measured through the multiplexer circuit. Tissue differentiation is still clear at high frequencies.

Therefore, if accurate EIS data is desired, it is recommended to have 100 kHz as an upper-frequency limit. If tissue differentiation is desired (such as surgical margin identification) frequencies up to 1 MHz may still produce useful measurements; however, as shown by Figure 31, the multiplexer introduces errors at that high of a frequency, so using such data for cross-sample comparison is not advisable. To justify the second prototype's ability to differentiate

between porcine muscle and fat at high (>100 kHz) frequencies, student t-tests were completed (Figure 33).

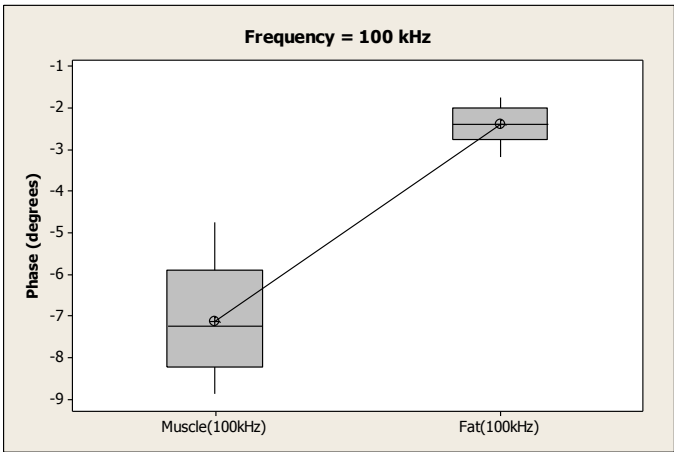

	N	Mean	StDev	SE Mean
Muscle(100kHz)	12	-7.11	1.30	0.37
Fat(100kHz)	10	-2.368	0.473	0.15

P-Value = 0.000
Means that the null hypothesis (that the two tissue have the same phase)is false.
Therefore muscle and fat have statistically different phase at 100 kHz.

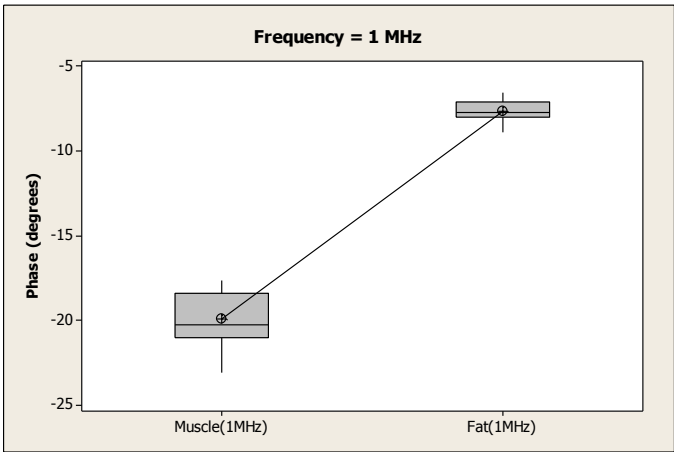

	N	Mean	StDev	SE Mean
Muscle(1MHz)	12	-19.86	1.62	0.47
Fat(1MHz)	10	-7.598	0.696	0.22

P-Value = 0.000
Means that the null hypothesis (that the two tissue have the same phase)is false.
Therefore muscle and fat have statistically different phase at 1 MHz.

Figure 33: T-test for the data reported in Figure 32.
At both 100 kHz and 1 MHz the muscle and fat have statistically different phase.

3.4.2 Low Frequency Noise in Agar Gel

Location-to-location variation had not yet been explored due to testing in only tissues of high heterogeneity. Agar gel was chosen because of its homogeneity to analyze the variability between locations on the same measurement (here measurement refers to the 26 individual measurements conducted by the second prototype probe). Additionally, the Agar gel

measurements were operated at a large frequency range of 10 Hz to 1 MHz, in order to compare the response in the homogenous material to the dummy cell measurements.

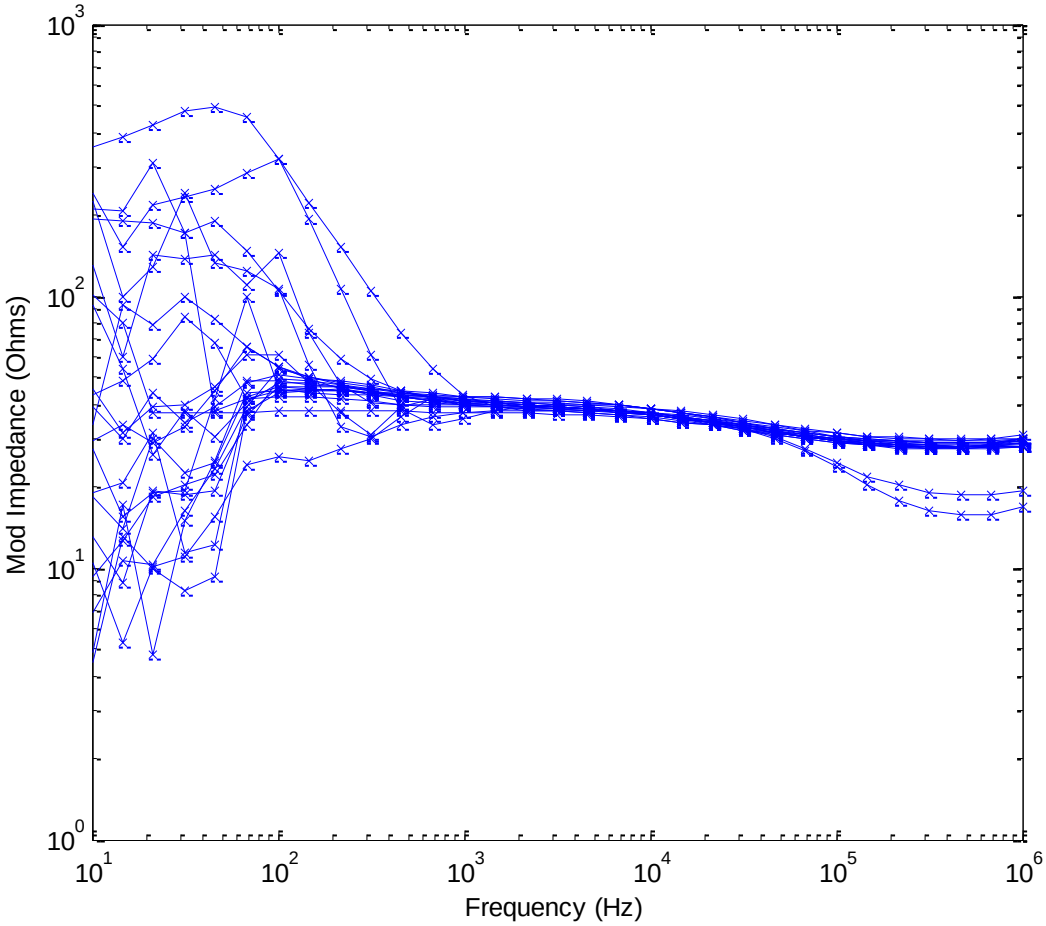

Figure 34: Low frequency noise observed in Agar gel.
Variance is seen at frequencies roughly less than 1 kHz. Different lines are different measurement locations within the second prototype probe.

Figure 34 shows that the multiplexer and/or probe interface may be introducing measurement error at lower frequencies. The consistency that is seen at higher frequencies does not remain at frequencies less than 1 kHz: some locations break smooth patterns and form jagged lines; others start to increase and then decrease rapidly. Since the Agar gel is a homogenous material and serves as the best-case scenario for tissue measurements, it is recommended to perform EIS

measurements at frequencies above 1 kHz. This low-frequency noise is hypothesized to be sourced from the probe itself and not the multiplexer, as the multiplexer matched the directly connected dummy-cell measurements at low frequencies. Perhaps a similar probe coated with a different material (current material Sn) would eliminate the low frequency error.

Since both low frequencies (< 1 kHz) and high frequencies (> 100 kHz) displayed deviations from expected impedance values, a middle frequency range is recommended for consistent EIS data that could be used to compare data cross-sample.

To test the consistency of the probe in this recommended frequency range, many measurements were conducted in Agar gel. EIS measurements in a homogenous material (Agar gel) would allow for the comparison of results from different locations within the probe. The probe can take 26 measurements without being translated, but should also display consistent results if moved within a homogenous sample. Figure 35 shows a photograph of the probe indentation left behind in Agar gel, illustrating how the probe was moved from location to location to test consistency across the homogenous sample. Figure 36 shows the results from the consistency experiment in Agar gel.

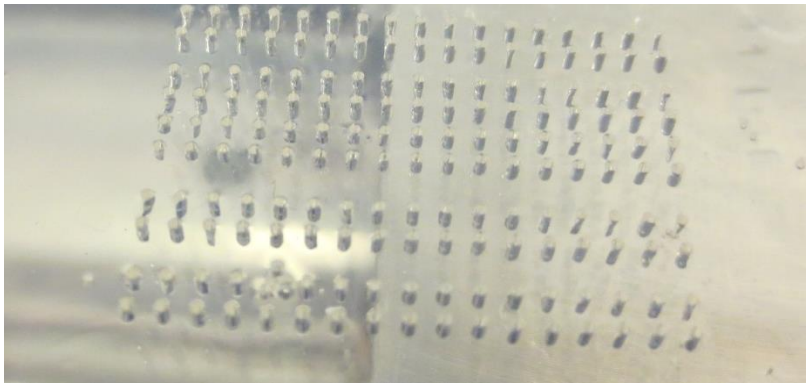

Figure 35: Probe indentation left behind in Agar gel.
To gauge measurement reliability in a homogenous material, the probe was translated to different places in the gel.

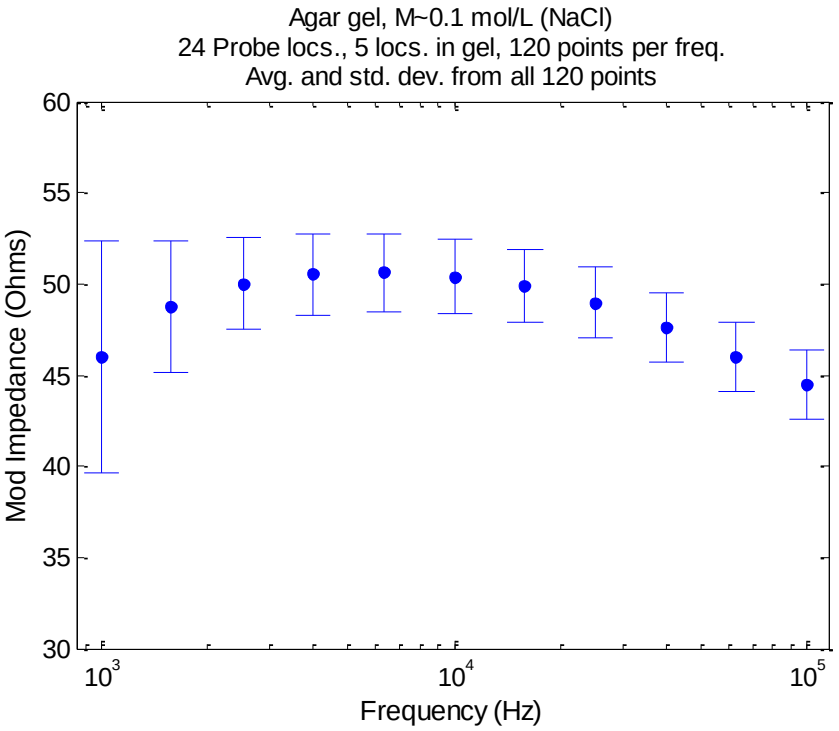

Figure 36: Measurement consistency in Agar gel.
Data was taken across different gel locations as well as different locations within the probe.

Table 3: Numerical data for Figure 36: measurements in Agar gel.

Frequency (kHz)	1.0	1.6	2.5	4.0	6.3	10	16	25	40	63	100
Mod Impedance (Ohms)											
Average	46	49	50	51	51	50	50	49	48	46	44
Std. Dev.	6.4	3.6	2.5	2.2	2.1	2.0	2.0	1.9	1.9	1.9	1.9
Range	31	20	15	12	12	12	12	12	11	11	11

The Agar gel measurements confirm the noise that begins to become visible at around 1 kHz: the range and standard deviation are a maximum at 1 kHz. At 4 kHz to 100 kHz, the range and standard deviation are mostly consistent at about 12 Ω and 2 Ω, respectively. Imaginary impedance as well as phase data had ranges and standard deviations that were similar in magnitude, and are thus not displayed. These values for standard deviation and range can be used as a baseline for expected repeatability of the probe for measurements in human tissue. The range caused by variability in the probe itself was measured to be about 12 Ω /50 Ω = 24% of the

average value in Agar gel. It would be reasonable to expect the same variability to occur in human tissue measurements as well: impedance should be able to be accurately measured within ±12% for human tissue measurements.

3.4.3 Multiplexer Ground Setup

While differentiation of tissue type could be achieved using data collected by the second prototype, it was observed that the data diverged from first prototype data at high frequencies (Figure 37). For example, first prototype real impedance data is concave down at high frequencies, while second prototype real impedance data is concave up. The phase data followed the same pattern, and reached high (> 20°) values, both positive and negative. Therefore it was hypothesized that the multiplexers may not have been in correct operation.

The following figures and discussions are a comparison of EIS data when the only variable changed was multiplexer ground/power connection. Initially, the multiplexer was powered/grounded to the Arduino Mega's power (5 V) and ground; however, it was thought that it may be advisable to instead power/ground the multiplexer to the measurement device itself (the potentiostat). The constant digital ON of the potentiostat is also at 5 V. Five volts is in the recommended voltage range for the multiplexer's operation, so the potentiostat should be able to sufficiently power the multiplexers.

Phase Data Comparison (Potentiostat/Arduino Grounded)

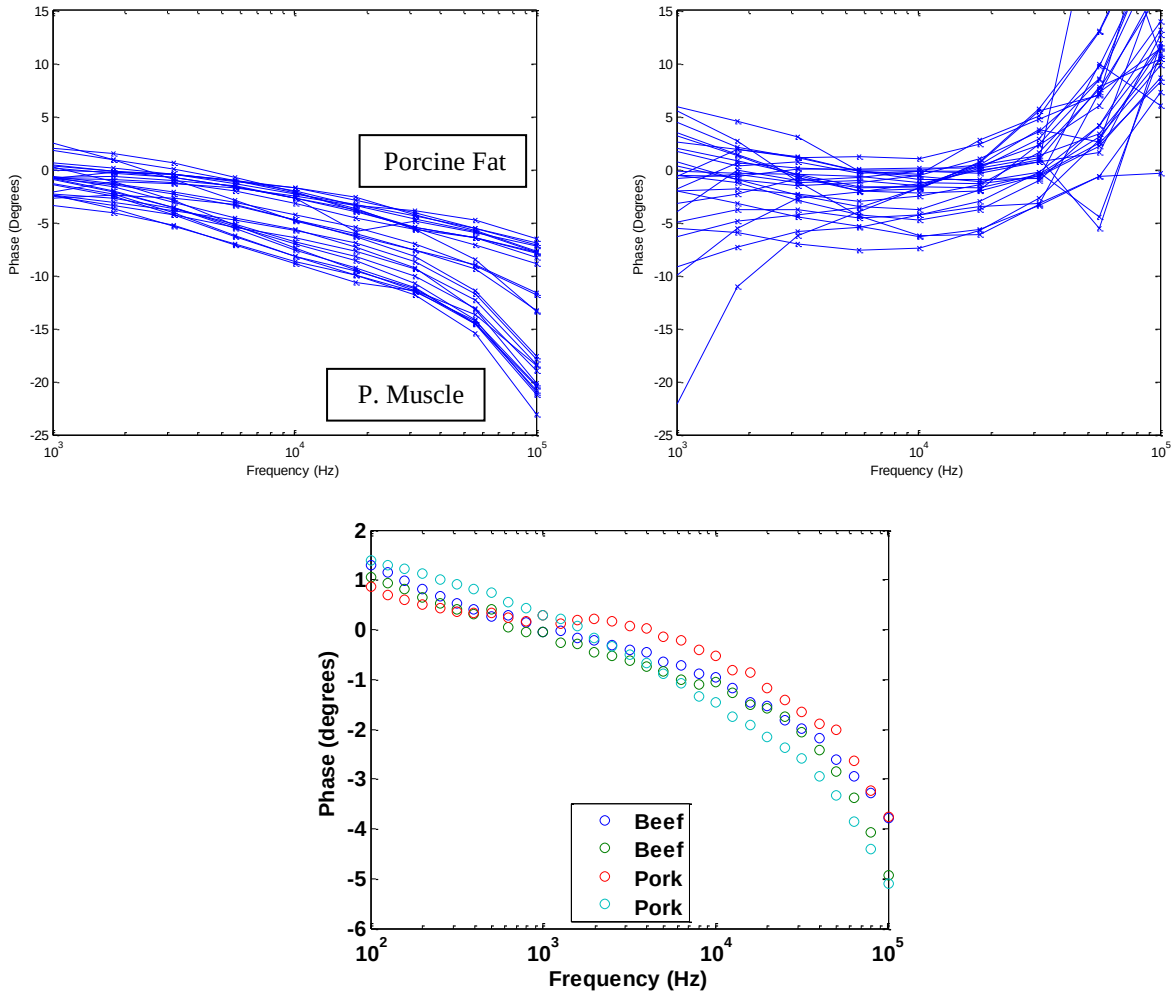

Figure 37: EIS phase data comparing ground sources.
Shows the change produced when switching multiplexer ground and power from the Arduino to the potentiostat. (Top-left) multiplexer powered/grounded by potentiostat. (Top-right) multiplexer powered/grounded by Arduino. (Bottom) for reference, data collected by first prototype, in the absence of the multiplexer IC.

Note that when the multiplexer was grounded/powered by the potentiostat, the data matched the overall shape of the first prototype data: both being concave down. Note that when the multiplexer was grounded/powered by the Arduino, the phase at high frequency became positive instead of negative. Additionally at higher frequencies, the potentiostat grounded/powered data diverges to separate values for the porcine muscle/porcine fat tissues, while it is difficult to

distinguish between tissue types looking at the Arduino grounded/powered data, as is shown at a single frequency (100 kHz) in the following figure.

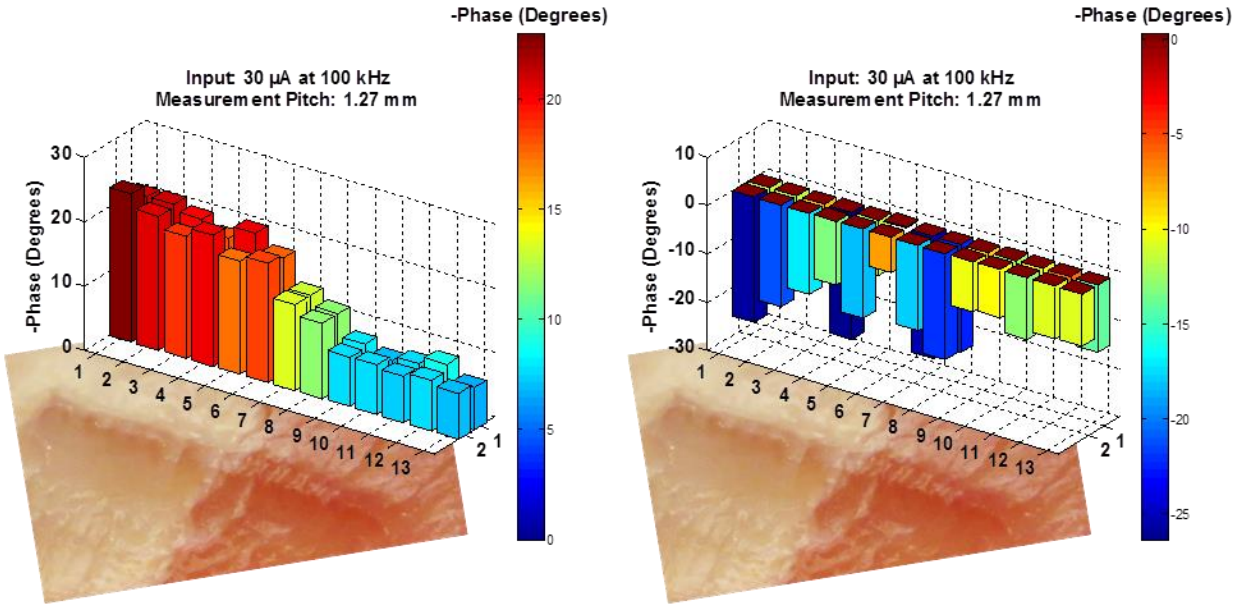

Figure 38: EIS image comparing ground sources, using phase data.
Data collected at (100 kHz). (Left) multiplexer powered/grounded to Gamry. (Right) multiplexer powered/grounded to Arduino.

Real Impedance Data Comparison (Potentiostat/Arduino Grounded)

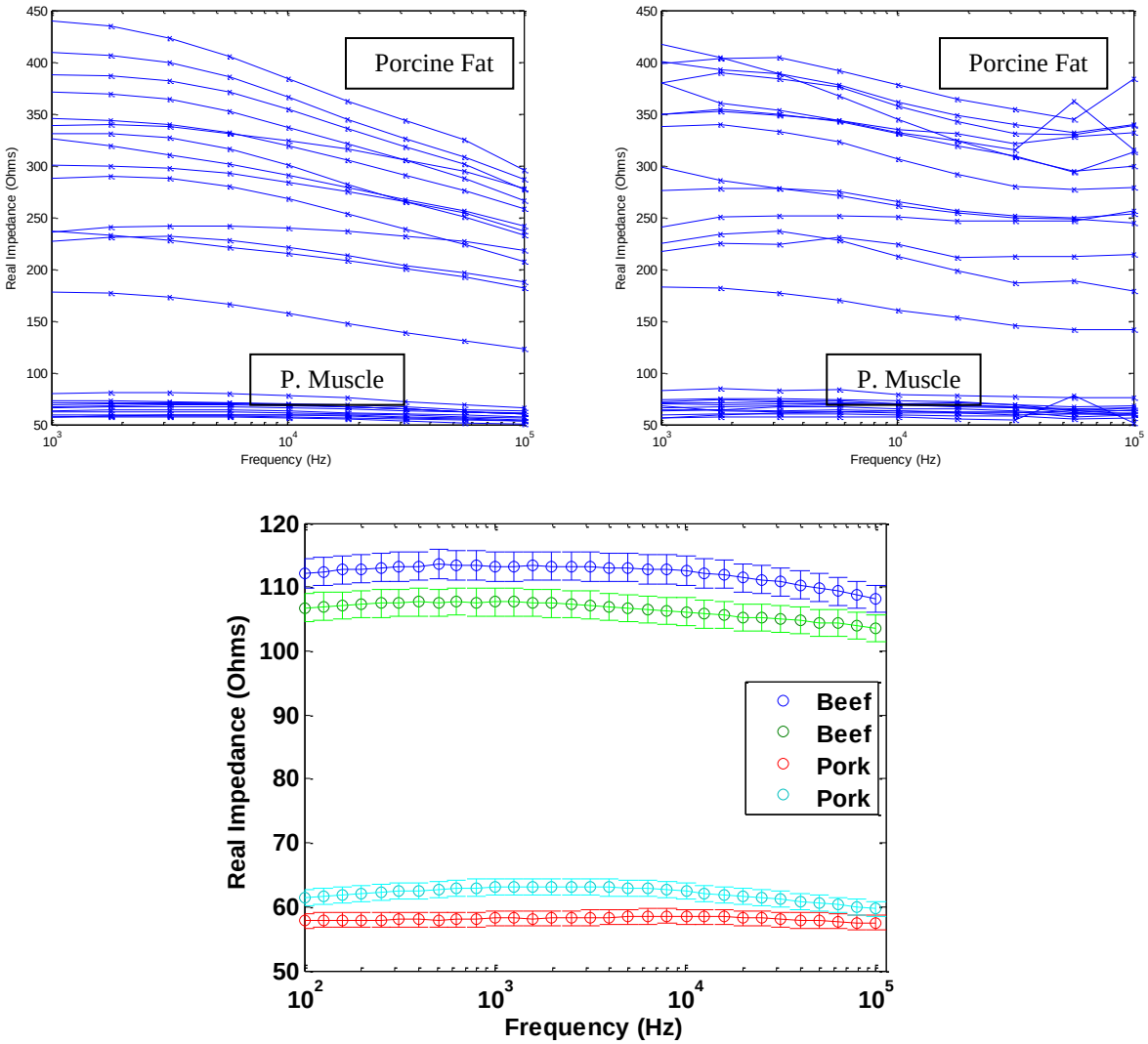

Figure 39: EIS real impedance data comparing ground sources.
(Left) multiplexer powered/grounded to potentiostat. (Right) multiplexer powered/grounded to Arduino. (Bottom) for reference, data collected by first prototype, in the absence of the multiplexer IC.

The real impedance data was not affected as much as the phase data by the switch in ground. Both the potentiostat-grounded and Arduino-grounded impedance curves follow the general trend of concave-down curves, with highest impedance at lower frequencies. However, some anomalies in the data do exist at high frequencies for the Arduino-grounded data. For example, at

100 kHz many locations in the porcine fat experience upward spikes in impedance instead of the decreasing trend experienced at other frequencies. If focusing in on only a single frequency (Figure 40), the potentiostat-grounded and Ardunio-grounded EIS measurements produced a similar ability to distinguish between porcine fat and porcine muscle. This observation is significant because the first tests ran on excised human liver samples was Arduino-grounded, as the effect of grounding had not been hypothesized at the time of the experiment.

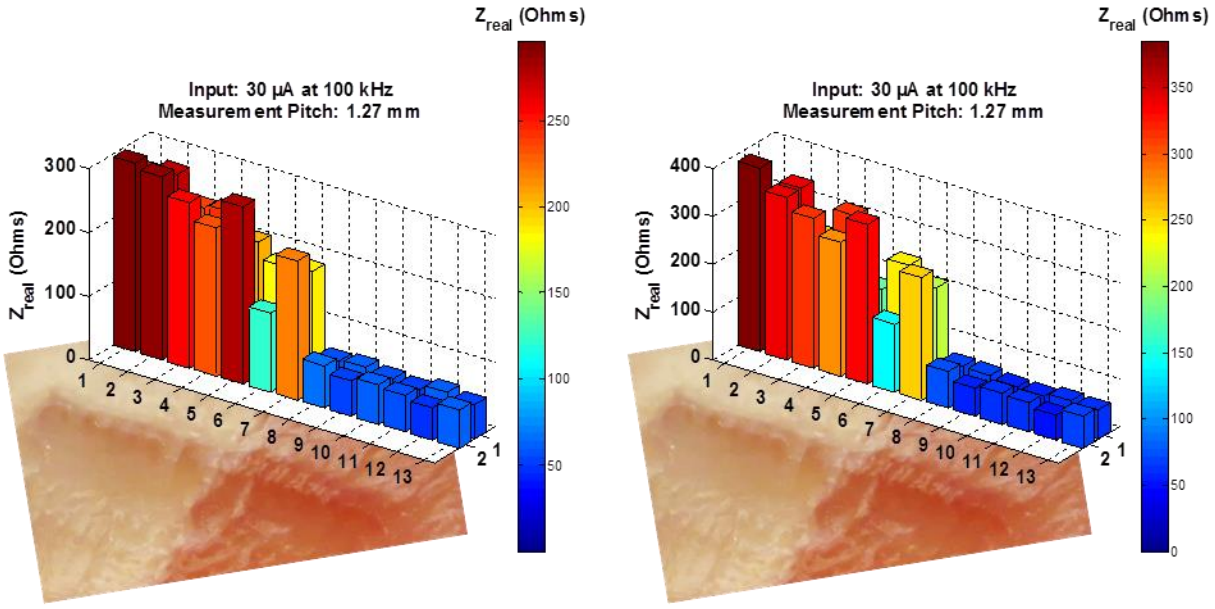

Figure 40: EIS image comparing ground sources, using real impdance data.
Data taken at (100 kHz). (Left) multiplexer powered/grounded to Gamry. (Right) multiplexer powered/grounded to Arduino.

Imaginary Impedance Data Comparison (Potentiostat/Arduino Grounded)

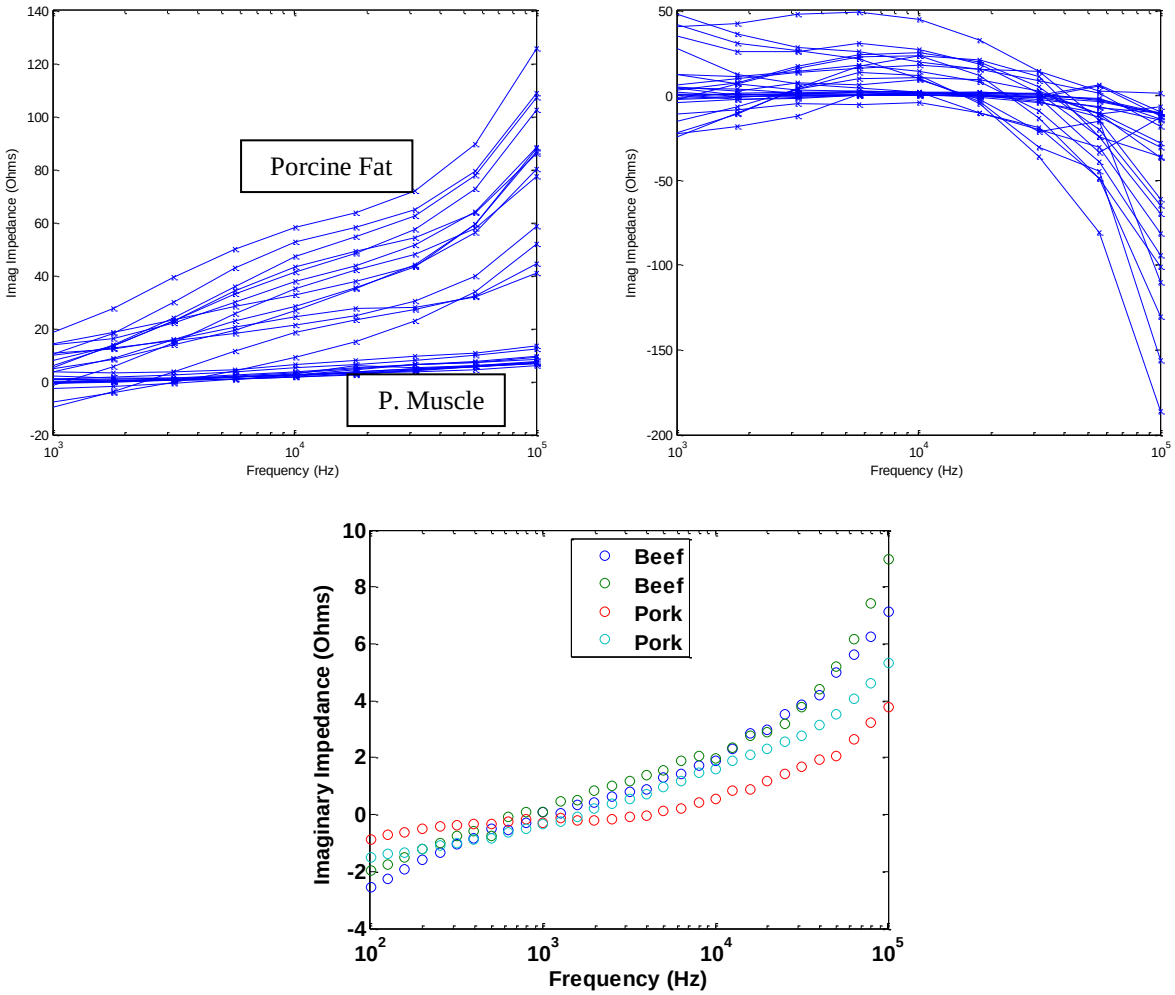

Figure 41: EIS imaginary impedance data comparing ground sources.
(Left) multiplexer powered/grounded to potentiostat. (Right) multiplexer powered/grounded to Arduino. (Bottom) for reference, data collected by first prototype, in the absence of the multiplexer IC.

The imaginary impedance, like the phase, was grossly affected by the change in grounding source (Figure 41). Also like the phase, the concavity of the curves reversed back to the concavity of the data collected by the first prototype when correcting the grounding source. This suggests a strong correlation between the phase and imaginary data, while the real data was more

unaffected by the change in ground. Figure 42 displays the imaginary impedance data as a single-frequency image.

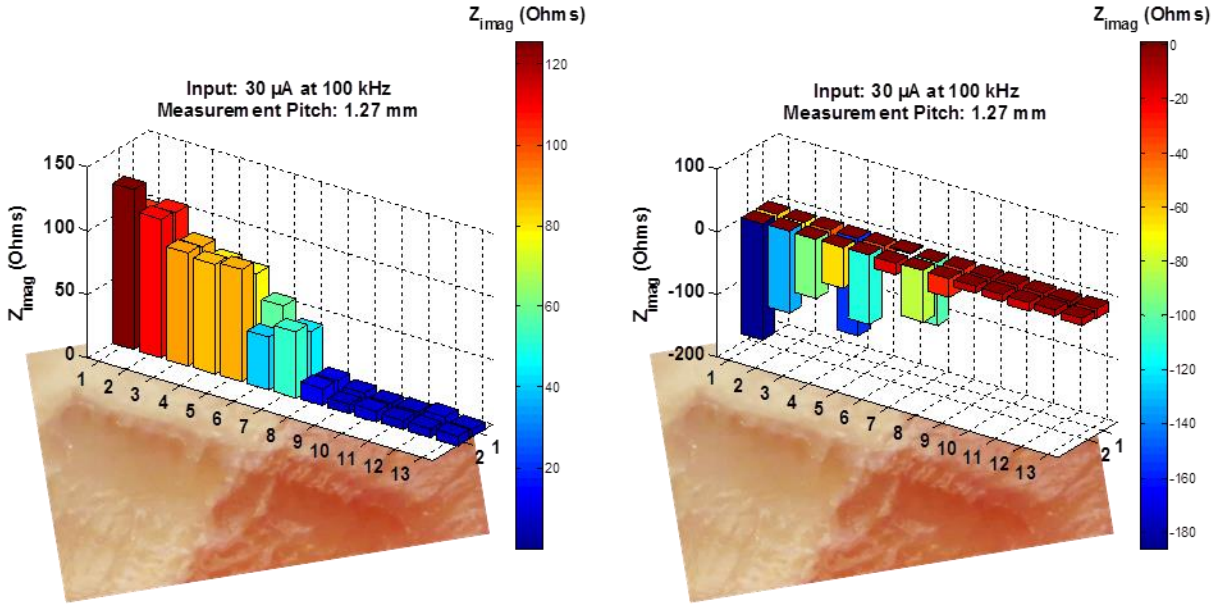

Figure 42: EIS image comparing ground sources, using imaginary impedance data. Data taken at (100 kHz). (Left) multiplexer powered/grounded to potentiostat. (Right) multiplexer powered/grounded to Arduino.

The impedance modulus data is not discussed in detail here because it follows very closely to the real impedance data. However, there is one more significant improvement that was observed when changing grounding sources: the ability to consistently run EIS measurements in the 100 kHz to 1 MHz range. When the multiplexer was connected to Arduino ground, the ability to take galvanostatic EIS measurements at frequencies above 100 kHz was often erroneous, quitting the measurement because of too large of current or voltage responses. However, it was noticed that this error no longer was experienced when switching the ground to the potentiostat. The following figure displays the faulty impedance reading that was generated at high frequencies when connected to Arduino ground.

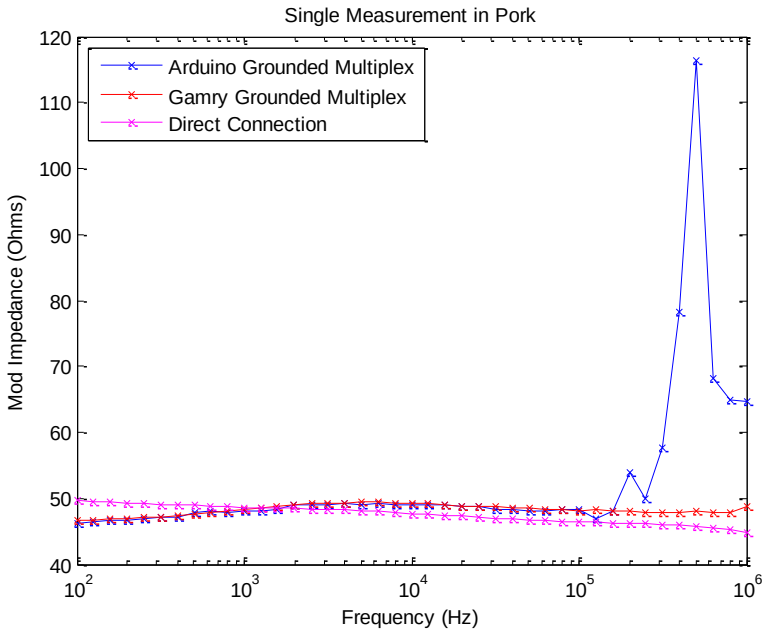

Figure 43: Noise between the 100 kHz and 1 MHz range caused by ground source. Noise is observed when ground connected to Arduino. 'Direct Connection' refers to the potentiostat inputs connected to the measurement probe with no intermediate multiplexer or switch.

This effect can be explained by the divergence of the imaginary part of the impedance at high frequencies, as was previously observed in Figure 41: the imaginary impedance was nearly 0 Ohms at low frequencies, but started to increase sharply at about 100 kHz. This effect is more pronounced in porcine fat tissue but less pronounced in porcine muscle tissue. Figure 43 was produced with data measured in porcine muscle, so the extremity of the error produced at high frequencies would be expected to be even higher if measured in fatty tissue.

3.4.4 Stacked Probe Uncertainty

Isolation of the microarray probe from cancerous tissue was a major concern for measurements conducted on human hepatic tissue; for safety precautions it was assumed that the tissue was infected with diseases such as HIV, Hepatitis B, etc. Therefore, any portion of the measurement device to make contact with the tissue would be discarded. However, the attachment of the 34-

pin microarray to the 2.54 mm wiring harness is a time-consuming and difficult procedure, so it was desired to keep this work preserved. An idea proposed (and used in the first measurements on human hepatic tissue) was to stack an identical probe onto the end of the measurement device (Figure 44) and then discard that probe after the measurements. Measurements in homogenous Agar gel were used to compare the non-stacked and stacked probe arrangements (Figure 45 and Figure 46, respectively).

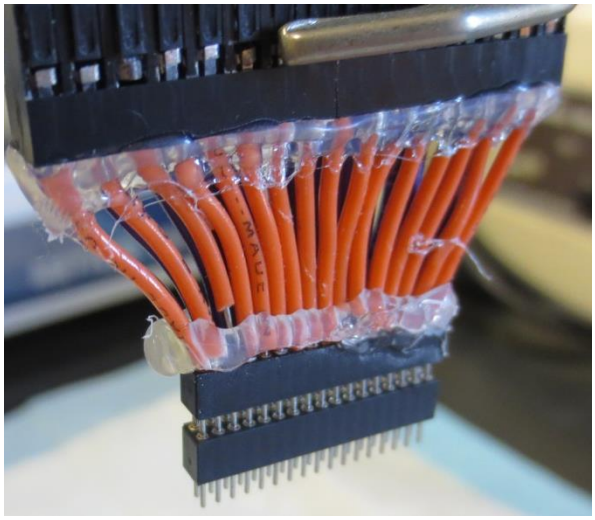

Figure 44: Stacked probes photograph.
This arrangement allowed easy removal of the exposed portion of the probe but may have caused large measurement error.

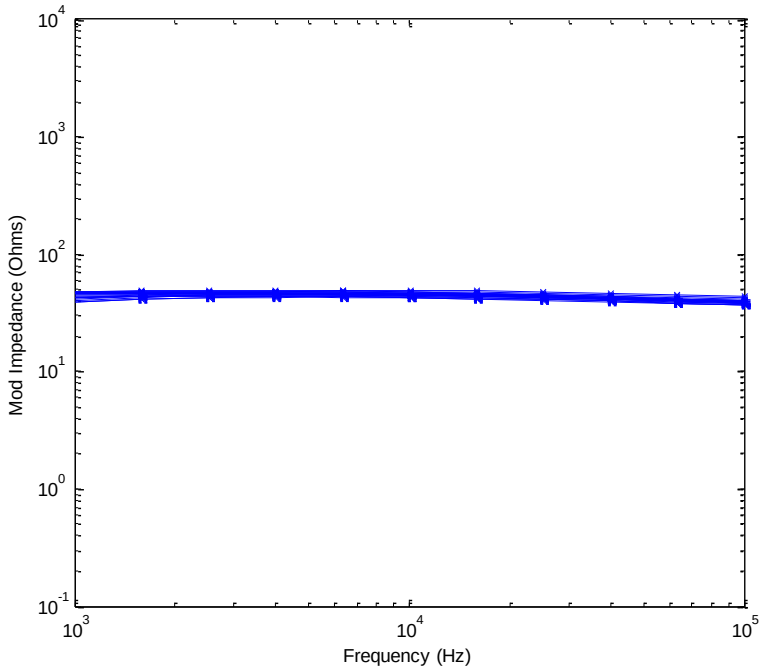

Figure 45: Galvanostatic EIS in Agar gel, using a single probe.
The 26 different lines (not visible here due to overlap) represent the 26 different locations taken in a single measurement.

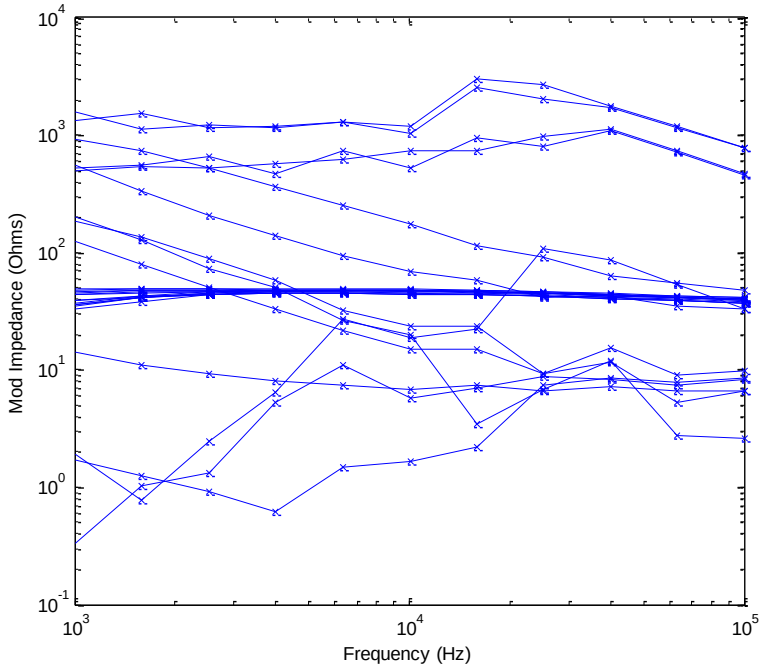

Figure 46: Galvanostatic EIS in Agar gel using the stacked probe arrangement.
12 of the 26 measurement locations showed responses different from those seen in Figure 45.

The measurements made in Agar gel show that the stacked probe arrangement has the potential to introduce much variability into the measurement. While Figure 45 (single probe arrangement) produced impedance modulus values between 40 and 50 Ohms, Figure 46(stacked probe arrangement) produced uncharacteristic EIS curves at about half of the locations: impedance modulus values ranged from a few kOhms to under one Ohm. While not all of the curves deviated so largely from the single probe arrangement, it is plausible that the stacking error could be propagated into important human-tissue measurements: therefore the stacked probe arrangement is not recommended.

CHAPTER 4. EX-VIVO HUMAN LIVER MEASUREMENTS

Permission to conduct EIS measurements on freshly excised human liver metastatic tissue was obtained through an IRB protocol. Human liver measurements were run in collaboration with a long-term study being directed by both the Prakash and Subramaniam groups. The goal of these measurements was to test the prototype's ability to distinguish between tumor/non-tumor human tissue. In all cases, a separate, smaller portion of human liver was sectioned specifically for measurements using the microarray prototype. Measurements were conducted in Wiseman Hall at The Ohio State University.

4.1 December 19, 2013 Case

It is important to note that the 12-19 case was conducted before any of the sources of error (presented in Chapter 3.4) were eliminated. However, displaying the data taken on 12-19 does a great job of highlighting the improvement to the measurement that was experienced when the sources of error were eliminated. Those sources of error include: the stacking of probes, incorrect grounding source for the multiplexer, and measurement deviation caused by the multiplexer at certain frequencies (< 1 kHz or > 100 kHz).

Extra care was taken to ensure that the human tissue never made contact with the measurement operator or to any part of the measurement device besides the probe interface itself. Besides extra safety precautions and the stacking of the probe, the actual measurement procedure was the same as that which was used for measurements in porcine phantoms or Agar gel. The probe was placed into roughly half tumor tissue and roughly half normal tissue. Then, with a single-click, the probe and multiplexer executed 26 serial EIS measurements across the tissue's surface. Figure 47 displays the sample used for the 12-19 case, while Figure 48 displays the results of the case across the entire measured frequency range.

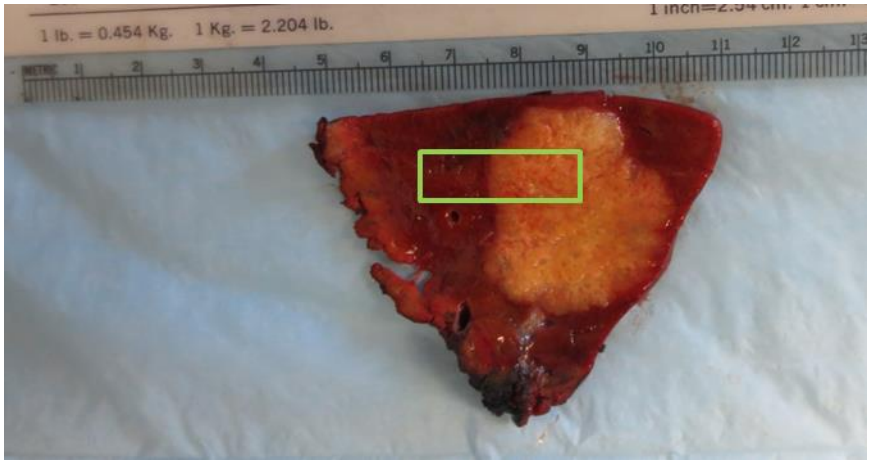

Figure 47: Human liver tissue from 12-19.
Tissue was approximately 6 cm by 6 cm in size. Thickness varied but was roughly 1 cm thick. White tissue is tumor while red tissue is normal. Green box indicates approximate location of the probe while measuring the data to follow.

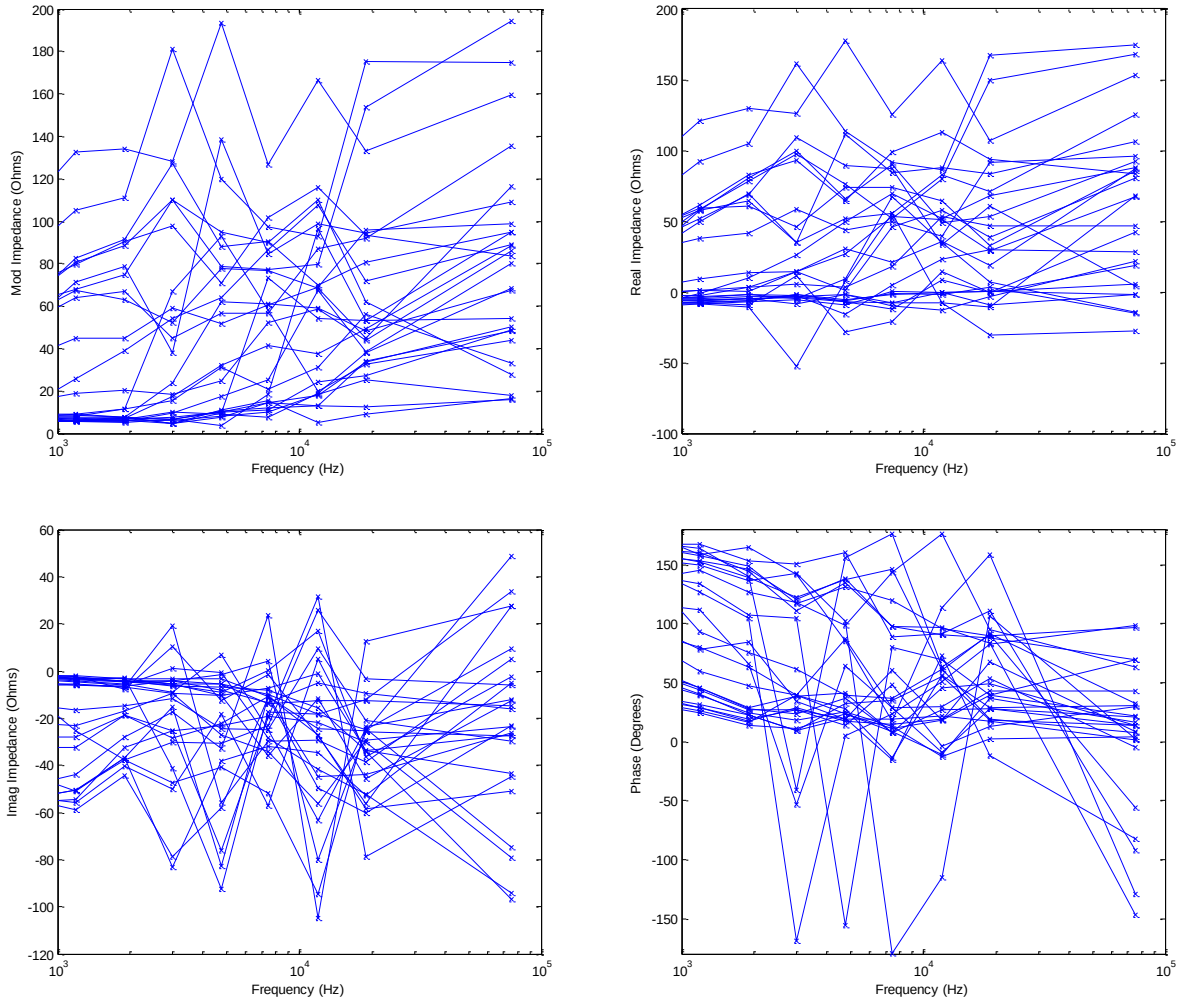

Figure 48: EIS data for 12-19 tissue, location B.
Data was collected before sources of error (such as incorrect grounding source and stacked probe arrangement) were removed.

The above figure shows many unexpected results. Abrupt changes in magnitude are observed in modulus, real, and imaginary impedances values. The phase even transitions from highly positive (more than 100°) to highly negative (less than -100°) in single frequency steps. At single locations within the probe, impedances bounce up and down, instead of following smooth trends. Negative impedances are seen in the real impedance chart. From these measurements, it was clear that something was wrong with the probe and multiplexer: accurate results could not be

obtained across the measured frequency range. Figure 49 shows the data presented as an image, using the modulus of the impedance at 1 kHz.

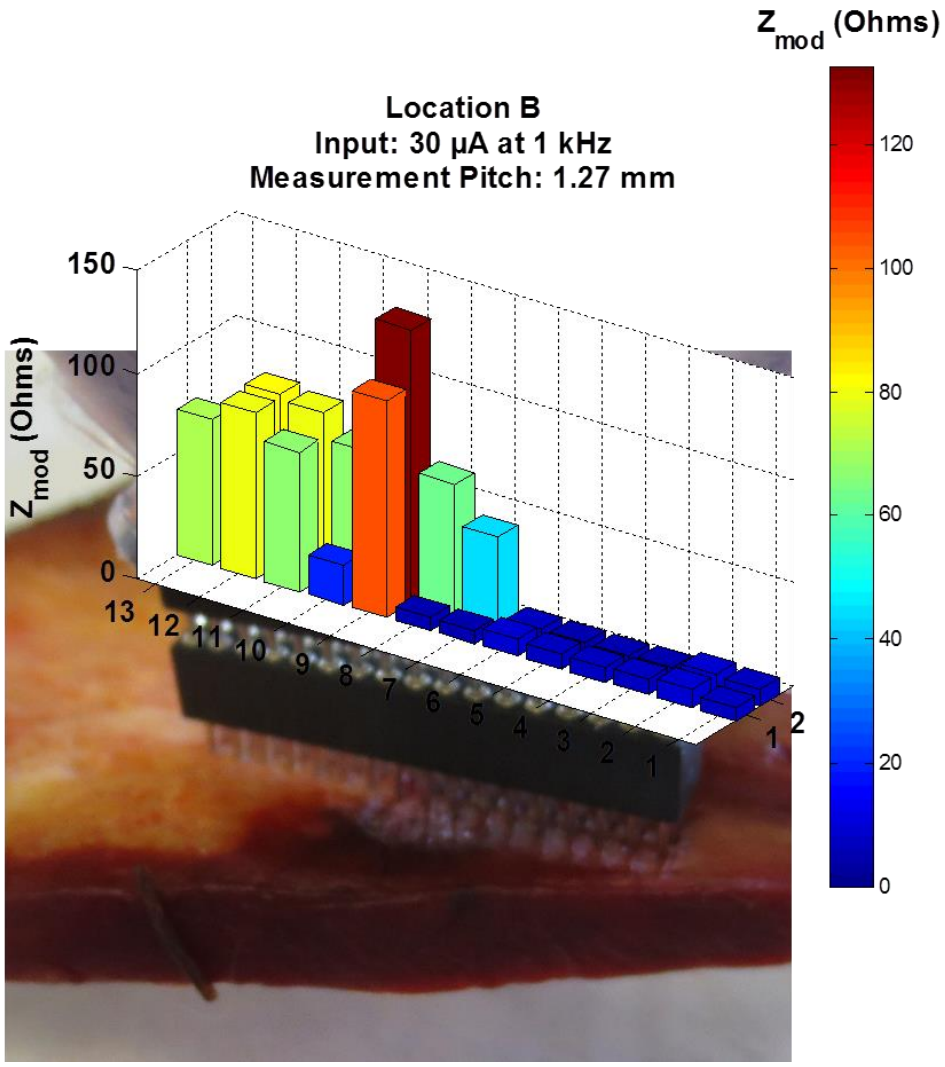

Figure 49: 3D bar graph image for 12-19 tissue.
Graph is overlaid on top of a digital image to show approximate location of impedance across the tissue surface. Here, the normal tissue has lower impedance, which was unexpected but may have been caused by the erroneous grounding source or stacked probe arrangement.

While previous studies have shown that hepatic tumor tissue should have lower impedance when compared to hepatic normal tissue (Haemmerich et al., 2009), the measurements taken on 12-19 are in disagreement. It is hypothesized that the measurement on 12-19 was severely affected by

the incorrect grounding source and the stacked probes (as was discussed in Chapters 3.4.3 Multiplexer Ground Setup and 3.4.4 Stacked Probe Uncertainty). While the actual values of the impedance or phase may not be correct, Figure 49 shows that the probe still could distinguish between tissue types. However, such a measurement would lead to the non-tumor region being identified as tumor and vice-versa.

As was previously mentioned, the measurements conducted on 12-19 were taken before any of the sources of error were eliminated (such as incorrect grounding source and stacked probe arrangement). The 12-19 case proved to be a good indication that such errors existed, and was a good first opportunity to test the probe and multiplexer on a real, excised human tissue sample.

4.2 February 12, 2014 Case

By the 2-12 case, the previously discussed sources of error were removed. The sample received on 2-12 was large enough in cross-sectional area, but was very thin (about 0.5 cm on average) and was slanted so that a measurement could not be easily conducted on a flat surface (recall the importance of consistent sample thickness as discussed in chapter 2). The probe was tilted in an effort to penetrate the pins an equal distance against the sloped tissue (Figure 50). Additionally, the boundary between the tumor and non-tumor tissue was less distinguishable as compared to the sample received on 12-19.

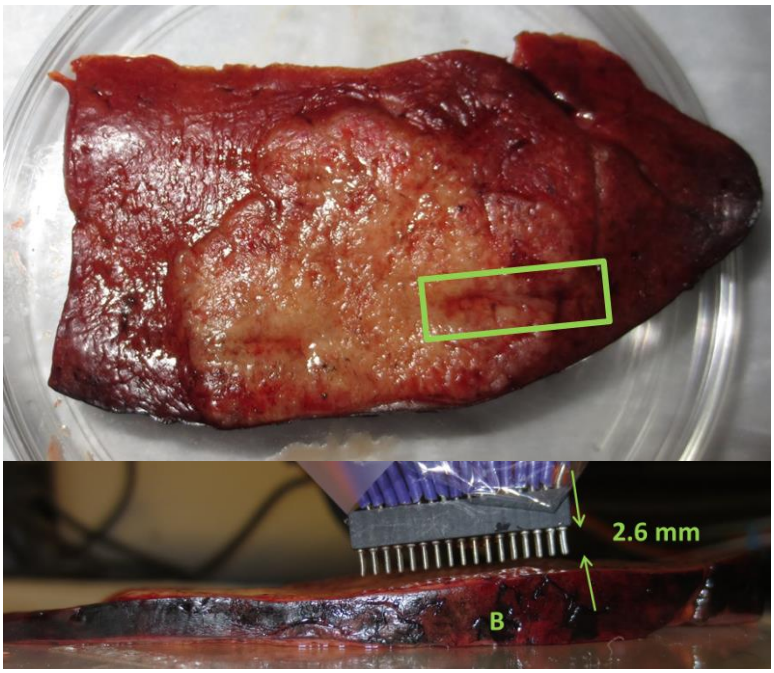

Figure 50: Top and side view of 2-12 liver sample.
Green box indicates approximate location of the probe while measuring the data to follow. The sample was about 8-9 cm long and roughly 0.5 cm thick.

Figure 51 shows the modulus, real, and imaginary impedances, as well as the phase, of the 2-12 liver at location B. For all sets of data, a visual difference can be seen between the tumor and non-tumor tissue. However, an outlier (highest impedance) exists which matches neither the tumor nor the normal tissue. The outlier is hypothesized to be caused by an extremely thin portion of the tissue, where the probe may in fact be protruding all the way through the tissue and touching the plastic surface beneath the tissue.

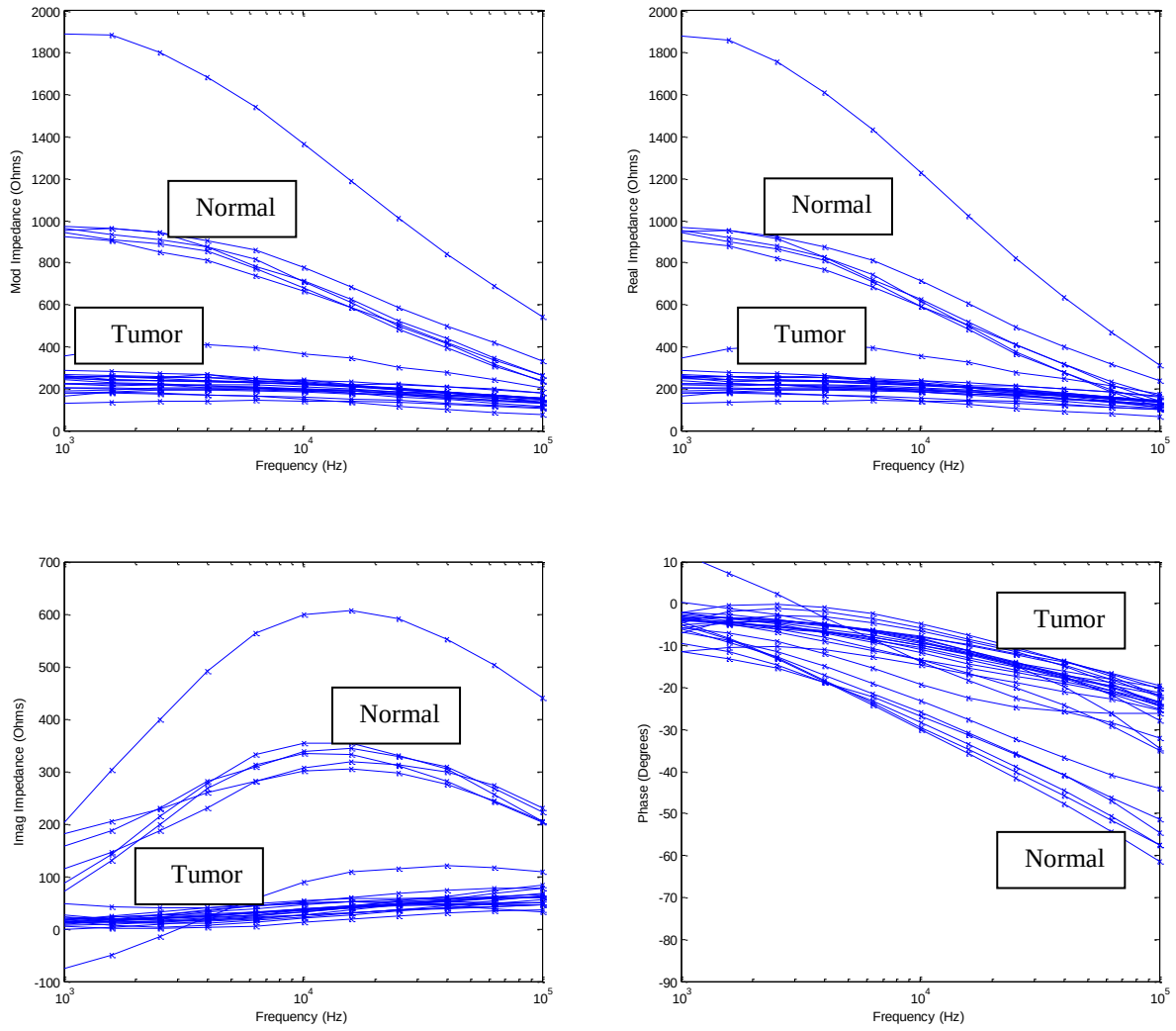

Figure 51: EIS data for 2-12 tissue, location B.
High-impedance outlier may have been caused by complete penetration of the thin tissue sample by one or more of the measurement pins.

Figure 52 is an image produced from the data displayed in Figure 51. All types of data were satisfactory for image generation and tissue differentiation; however, images were produced from only the modulus of the impedance as well as phase data.

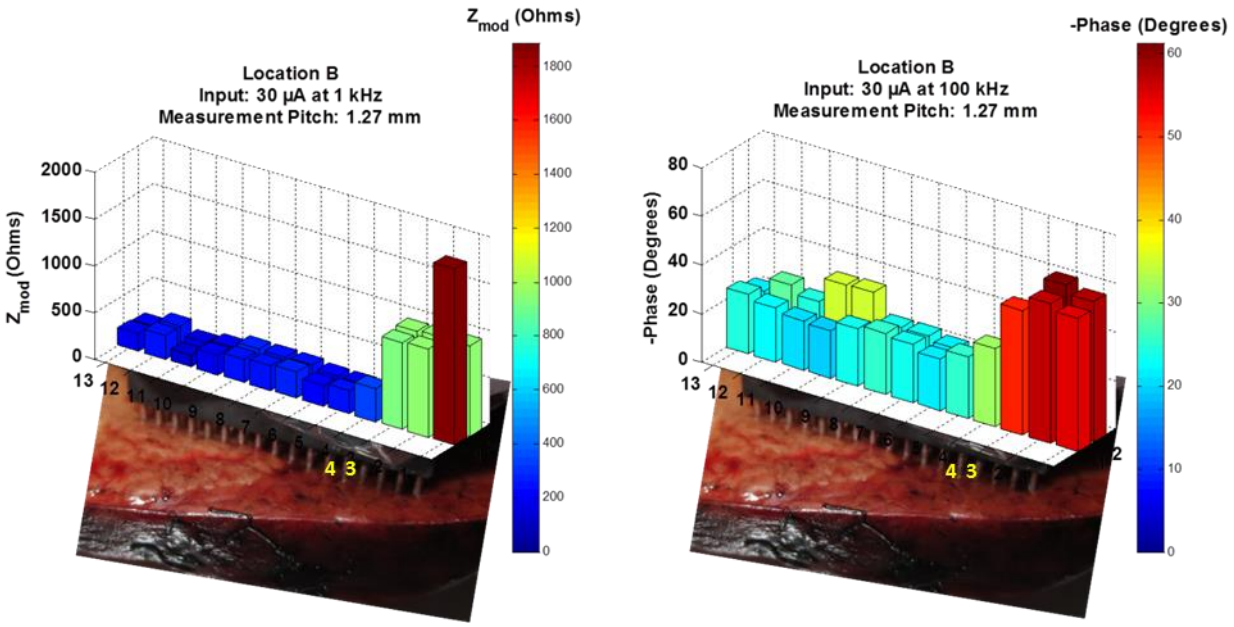

Figure 52: 3D bar graph images for 2-12 tissue.
Highest difference in impedance observed at lowest frequency (1 kHz, left) while highest difference in phase observed at higher frequency (100 kHz, right). The yellow 4 and 3 are the approximate locations of measurements 4 and 3, and are used in the discussion of the last paragraph of this section.

Unlike the case on 12-19, the 2-12 case produced smooth impedance curves at all probe locations. Figure 53 illustrates the improvement produced by removing the stacked probe and grounding source errors.

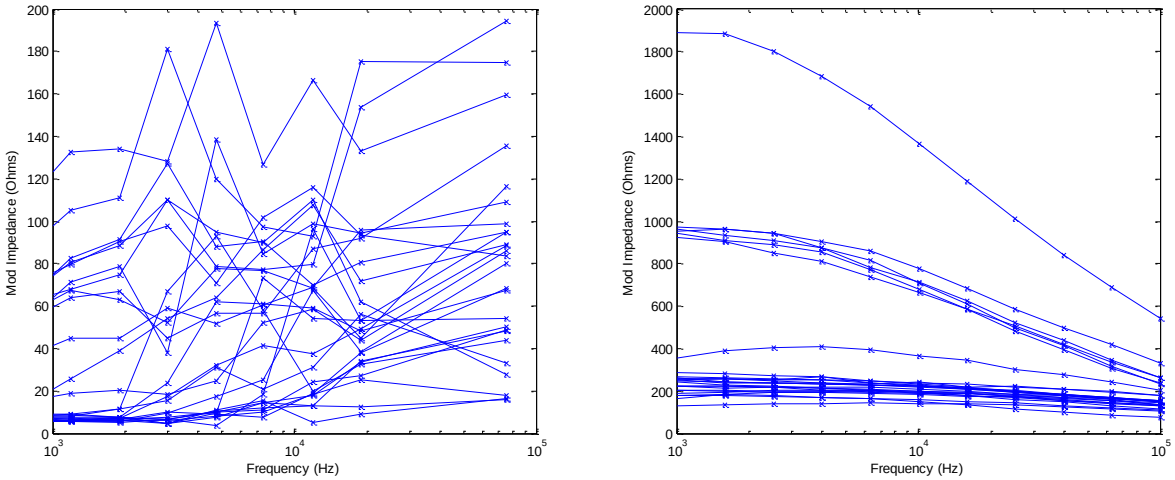

Figure 53: December 19 (left) vs. February 12 (right) impedance modulus.
Notice the improvement in the measurement after sources of error were removed. Now a clear difference between tissue types may be seen, and all jaggedness is removed.

The thickness of the tissue on the 2-12 case is expected to have negatively influenced the measurement. Location B (from which data was reported) was the best-case of the four measurement locations tested at. Other locations were too thin and produced erroneous results, which are believed to be caused by pins which actually penetrated the tissue and touched the platform surface beneath (plastic).

Additionally, it is difficult to discern the exact transition from normal to tumor tissue on the 2-12 sample using digital photography. Therefore it is not possible to reliably match the sharp impedance/phase transition seen between positions 3 and 4 (Figure 52) to the digital image of the tumor/non-tumor interface. While it was attempted to place half of the probe in each of the two tissue segments, the data shows only 3 of the 13 (in each row) measurement locations being clearly different from the remaining 10 (in each row). However, the sudden change in either phase or impedance is seen in all data types between positions 3 and 4 (Figure 52), suggesting that the actual transition between tissue types occurs somewhere between the 1.27 mm gap

between the centers of measurements 3 and 4. It is possible that although the surface of the tissue appears to be healthy at locations 3 and 4, the tumor is actually beneath the surface at those locations.

CHAPTER 5. DISCUSSION AND FUTURE WORK

In this chapter, the prototype's current functionality will be compared to two different EIS techniques. The first comparison will be to the translating technique that is in current use by the Prakash group, which uses a three-axis stage to move a single probe to different locations in the tissue. The second comparison will contrast the pin-switching logic of an already-patented electrical impedance measurement technique to the pin-switching logic of the microarray probe.

5.1 Microarray Probe Comparison to Translating Techniques

This section will compare the microarray probe with the current translating technique in regards to parameters that are important for implementation of the tool as a device that can assist surgeons during the identification of the surgical margin. These parameters include physical size of the measurement system, time of measurement collection (for image generation), and measurement resolution.

The microarray probe currently occupies a tabletop space of about 225 cm^2 (15 cm x 15 cm). While this area could very well be cut in-half through the construction of a custom printed circuit board, it nonetheless illustrates the potential of how small the non-translating EIS device can become. While the single probe and three-axis stage requires a large, sturdy lab bench and permanent fixture (non-mobile), the microarray probe's supporting electronics could easily be placed on the hip of a surgeon, allowing him/her the flexibility to move while using the tool. Figure 54 shows a size comparison of the two techniques.

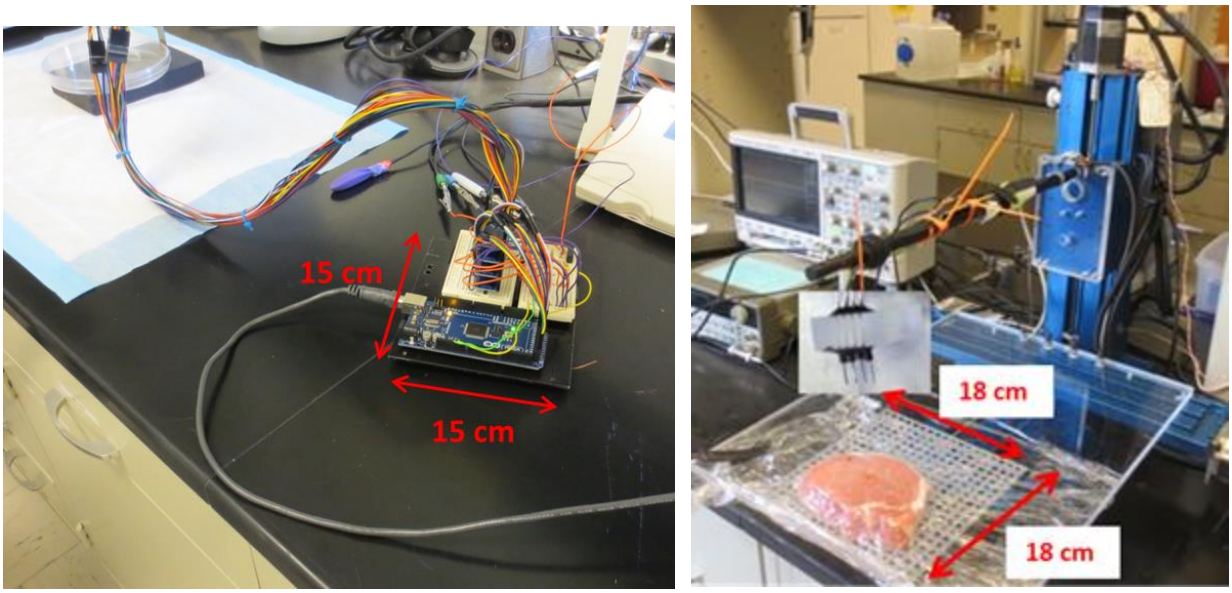

Figure 54: Size comparison of microarray probe and single probe setups.
(Left) microarray probe supporting electronics occupies an area of about 225 cm^2. (Right) translating stage of single probe setup occupies a large tabletop space. The dimensions of the microarray probe setup (15 cm by 15 cm) is smaller than the portion of the table reserved for samples (18 cm by 18 cm).

The time required to collect the array of EIS data needed to generate an image of the tumor/non-tumor interface needs to be as small as possible. Ideally, the device would generate the image of the tissue interface in real-time, allowing the surgeon to instantly confirm a surgical margin. However, true real-time tumor imaging is not possible using a single potentiostat, as the main contributor to the time of the overall measurement is repeating the potentiostat reading at different locations in the tissue (regardless of translating or non-translating techniques). While true real-time imaging is not possible, the device would still be useful for surgical margin verification if the image could be generated on the order of a few seconds.

The current time required by the microarray probe to take the 26 serial EIS measurements is 2 minutes and 30 seconds. However, half of that time is wasted by the potentiostat, when it idles for three seconds between each measurement. Since there are 25 measurement transitions, the saved time (if the idle period were removed) could be 75 seconds: reducing the total

measurement time to 1 minute and 15 seconds. Removing the idle-time in-between measurements could be achieved by modifying the sequence script file that the Gamry software defaults to. This was quickly attempted but to no success, as a decent background of the software language the Gamry script uses is required. The 1 minute and 15 second potential measurement is a large improvement over the translating technique, which takes anywhere from 30 to 90 minutes, depending on the number of points to measure and the speed in which the operator maneuvers the three-axis stage. While the 30 to 90 minute window is too long for a surgeon to modify his interpretation of a surgical margin, an image taking about a minute to generate should be quick enough for a surgeon to have the opportunity to verify the margin and make any recommended surgical margin changes, if desired.

Much of the work of the microarray probe was in design and construction of the multiplexer. While commercially available multiplexing solutions do exist, the multiplexer built here was designed specifically for use in conjunction with a 4-input potentiostat. Any commercial multiplexer would need to have the ability to have at least four inputs which can be multiplexed to any output. Additionally, the multiplexer made in-house was much more cost efficient than other solutions, being produced for less than $150 (depending on current prices of off-the-shelf components) while commercial multiplexers were found to cost upwards of $3700 (as compared to Agilent Technologies E8460A reed relay multiplexer).

The resolution of the microarray probe is currently defined as the pin-pitch of the pin array. The device built thus far has shown the ability to improve the resolution from 5 mm (translational technique) to 1.27 mm (the pin-pitch of the second prototype probe). The resolution of future micro-fabricated probes could be improved to sub-millimeter, limited by the micro-fabrication technique used and the durability of small-diameter electrodes. Such probes should be able to

identify surgical margins to less than 1 mm resolutions, which is the critical length-scale between sufficient and in-sufficient surgical margins as defined by Pawlik et al., 2005.

5.2 Microarray Probe Comparison to Patent US 8262575

A patent search was conducted to find similar systems which use electrical impedance spectroscopy measurements to identify cancerous tissue. In comparison to patent US 8262575 (Davies, 2012), the microarray probe switching technique allows for unique measurement reference points due to pin stepping and flexible pin operation. Pin stepping refers to the method previously discussed in which for each subsequent measurement the next pin serves the role of the previous pin (as if the pins were translated over by one pin pitch). This means that each measurement has a unique center arising from unique pins. In contrast, the electrode setup of patent US 8262575 uses a fixed "current passing electrode" in the center of the measurement (see Figure 55). In that arrangement, *all* measurements are tied back to the center electrode, so impedance measurements will always be in at least some ways characteristic of that center region of tissue. Using the microarray probe logic, the current passing electrodes are different for each measurement, and thus are not always tied to the center region of tissue where the "current passing electrode" lies.

Additionally, the flexible pin operation used in the microarray probe logic enables more measurements to be conducted using the same number of pins. Figure 55 illustrates this idea. Eight measurements are possible using the microarray probe logic (with centers-of-measurement seen as triangles) using 13 pins, while only half (or four) measurements can be conducted using 13 pins using the logic presented by patent US 8262575.

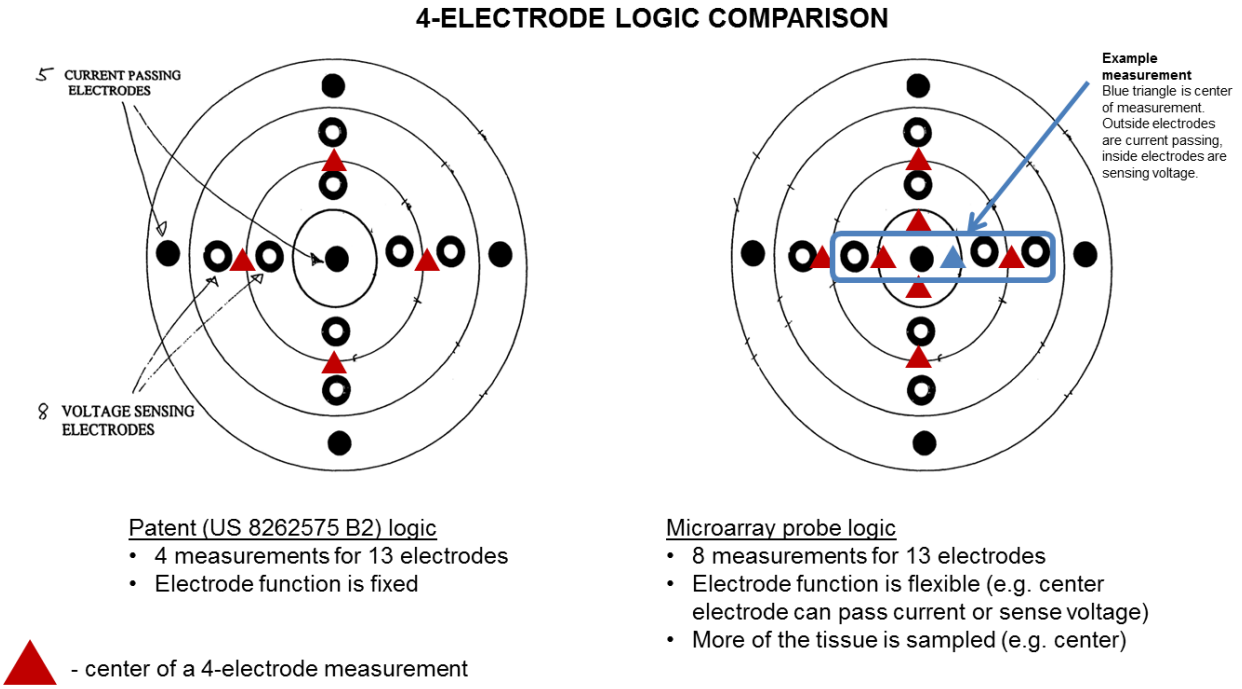

Figure 55: Logic comparison between patent US 8262575 and microarray probe.
Figure adapted from patent US 8262575 (Davies, 2012). The microarray probe allows for more measurements using the same number of pins (twice as many in this particular pin configuration), and allows each measurement to have its own, unique reference point.

5.3 Future Work

The microarray probe measurement system could be more feasibly implemented into a clinical environment after micro-fabrication of a custom probe and after design/construction of a custom printed circuit board.

The microarray probe was very limited in function due to the reliance on manufactured solutions for a probe interface. For example, the first prototype probe featured a large section in the center of the probe which did not contain any pins. This meant that the probe would never be able to generate a full image across the entire area of the probe. With the second prototype probe, the pins were organized with 17 pins in one direction and only two pins in the other, resulting in a long, skinny rectangle for an imaging area instead of a square, which would be desired. The

probes were obtained in these less-than-perfect configurations because they were the best solutions that could be commercially bought: large, square arrays containing pins across the entire area could not be found as an off-the-shelf component, despite exhaustive searching. A micro-fabricated probe would enable 1) a square array with no missing pins, enabling complete images that are identical in both height and width, 2) a smaller pin-pitch (likely on the order of tens of μm instead of mm), limited by the micro-fabrication technique and the desired pin durability: increasing the resolution of the image produced, 3) more (> 26) possible measurements, enabling images to survey larger portions of tissue, and 4) smaller form factor, enabled by the smaller pin pitch, and allowing the device to more easily fit onto the fingertip of surgeons.

A custom printed circuit board would enable the device to be more easily integrated into a portable surgical tool. While the second prototype of the microarray probe could fit onto the hip of a surgeon, it cannot yet fit onto the hand of the surgeon. Perhaps with a custom printed circuit board, the device could actually fit onto the dorsal side of the surgeon's hand. A glove could be produced that would contain the electronics on the top of the hand and the probe on the fingertip. Additionally, a custom printed circuit board may be necessary for increasing the number of measurements beyond 26. The existing integrated-circuit multiplexers are limited to 32 channels: when increasing the number of measurements past 32, more multiplexers (or multiplexers of higher channel capacity) will be required.

Other measurement factors that should be taken into consideration during future iterations of the device would be a method of detecting the force applied to tissue surfaces when in contact with the microarray, as well as variations in tissue impedance due to changes in sample volume. Although it is outside the scope of this particular thesis, it has been observed that measured

impedance is affected by the depth of penetration (if any) of the active electrodes into the tissue sample. Therefore, a sensor that could correlate force on the microarray to a depth of penetration might be able to add a correction factor to measurements of different contact force/electrode penetration. As sample thickness was shown to affect measured impedance values in the second chapter of this thesis, further studies into varying sample volume are recommended if attempting to make sample-to-sample comparisons of tissue impedance as measured by a multiplexed microarray system.

CHAPTER 6. CONCLUSION

A surgical tool prototype was designed, built, and tested. The microarray probe was designed with a unique method of multiplexing measurements. Compared to previous array probes, the microarray probe defines a local reference point for each measurement: past designs may use common current-injection electrodes, meaning that each measurement shares a common reference point. Measurements taken by the microarray probe each have their own unique reference point and are thus free from influence of past/future measurements. Compared to translating probe techniques, the microarray probe requires no physical movement, meaning that it requires no large machinery, can generate images of tissue interfaces in minutes instead of hours, can avoid errors arising from probe translation, and can potentially fit onto the hand of a surgeon.

Two prototypes were built. The first prototype was capable of multiplexing four measurements and did not incorporate any type of pin flexibility, i.e. four unique pins were required for each measurement. The second prototype was capable of multiplexing 26 measurements, and incorporated pins that could be flexible in function, allowing the spacing between measurements to decrease from four times the pin-pitch to one times the pin-pitch. Through the use of a microcontroller and multiplexer array, the second prototype displayed an ability to take measurements over an area swiftly and without user interaction – important traits for a surgical tool.

The microarray probe showed a strong ability to distinguish between both phantom tissues (porcine/bovine) and human hepatic tissue (tumor/non-tumor interface). Images of tissue interfaces were generated in just over 2.5 minutes from 26 serial EIS measurements, at the click of a single start button. The distance between subsequent measurements was decreased from

5 mm (single, translating probe) to 1.27 mm (microarray probe), meaning that a more precise surgical margin can be defined with the new tool. The probe itself is just over 2 cm long, meaning that it could easily fit onto the fingertip of a surgeon, and the supporting electronics can fit into a roughly 15 cm x 15 cm area. The small size of both the probe and supporting electronics means that the design has a high potential of being easily incorporated into the surgery room. Overall, the microarray probe in its current state serves as a proof-of-concept for a small form-factor, integrated EIS measurement device that can generate images of the tumor/non-tumor interface and thus allow a surgeon to verify the surgical margin in near real-time.

Future prototypes may incorporate micro-fabrication techniques to make a microarray probe designed specifically for use as a tissue-interface imaging device. This would enable smaller pin-pitches (increasing resolution) and would allow for a larger array of pins (increasing maximum number of measurements). A custom printed circuit board could incorporate all of the necessary electronics into a chip that could fit onto the dorsal side of a surgeon's hand. The custom manufactured microarray probe and printed circuit board would allow for realistic implementation of the device as a surgical tool that could assist a surgeon in verification of the surgical margin, and could therefore lead to more successful tumor resection surgeries.

BIBLIOGRAPHY

Cady, B., Jenkins, R. L., Steele, G. D., Lewis, D. W., Stone, M. D., McDermott, W. V., et al. (1998). Surgical margin in hepatic resection for colorectal metastasis: a critical and improvable determinant of outcome. *Annals of Surgery*, 227: 566-571.

Davies, R. J. (2012). *Patent No. US8262575 B2.* United States.

Dean, D., Ramanathan, T., Machado, D., & Sundararajan, R. (2007). Electrical impedance spectroscopy study of biological tissues. *Journal of Electrostatics,* 66:165-177.

Fricke, H., & Morse, S. (1926). The Electric Capacity of Tumors of the Breast. *The Journal of Cancer Research,* 10:340-376.

Gamry Instruments Incorporated. (2014, February). *Basics of Electrochemical Impedance Spectroscopy*. Retrieved from www.gamry.com.

Haemmerich, D., Schutt, D. J., Wright, A. S., Webster, J. G., & Mahvi, D. M. (2009). Electrical conductivity measurement of excised human metastatic liver tumours before and after thermal ablation. *Physiological Measurement,* 30:459-466.

Pawlik, T. M., Scoggins, C. R., Zorzi, D., Abdalla, E. K., & Andres, A. (2005). Effect of Surgical Margin Status on Survival and Site of Recurrence After Hepatic Resection for Colorectal Metastases. *Annals of Surgery*, 241:715-724.

APPENDIX A - PROCESS SHEETS

A.1 SC1 Clean

1. Fill a beaker with approximately 100 mL of deionized water.
2. Add 10 mL of hydrogen peroxide to the DI water.
3. User a micropipette, add 1 mL of ammonium hydroxide to the DI water solution.
4. Place beaker onto a hotplate and heat solution to 73°C, monitoring the temperature with a thermometer.
5. Once the temperature of the solution has reached 73°C, place the part to be cleaned into the solution. Try to maintain temperature at 73°C.
6. Wait for at least 10 minutes while the part is cleaned.
7. Remove part, rinse with water, and dry.
8. Turn off hot plate.
9. Dispose of solution into buffer waste.
10. Clean glassware and return to storage.

A.2 Connecting Gamry Potentiostat to Multiplexer

1. Turn Gamry ON.
2. Keep track of time: let Gamry stabilize for 30 minutes before taking any measurements.
3. Connect Arduino Mega to PC via USB.
4. ORANGE wire on pin 43 of TOP breakout board to Gamry GREEN alligator clip.
5. PURPLE wire on pin 43 of 2ND breakout board to Gamry BLUE alligator clip.
6. ORANGE wire on pin 43 of 3RD breakout board to Gamry WHITE alligator clip.
7. PURPLE wire on pin 43 of BOTTOM breakout board to Gamry RED alligator clip.
8. Gamry digital GROUND (pin 5) to reed relay center connection, on breadboard (should also be connected to 4 purple wires: the ground of the multiplexers, pins 23/24 on breakout boards).
9. Gamry digital HIGH (pin 15) to multiplexers power on breadboard (4 orange wires, connected to pin 14 of breakout boards)
10. Gamry digital D0 (pin 7) to other reed relay center connection, on breadboard, and creating no node with other wires.
11. Gamry BLACK alligator clip to earth ground. This connection is not required but should reduce measurement noise.
12. If probe head is not connected, connect to extension wires. There are three 12-pin extension wire harnesses. The color of the wires should match between harnesses.

A.3 Running an EIS Measurement (Gamry/Arduino Loops)

1. See process sheet A.2 for measurement device preparation (connecting potentiostat to multiplexer).
2. Open Arduino code titled Second_Prototype_Script.ino.
3. Make sure correct Arduino is identified by the software. Go to Tools>Board and select Arduino Mega 2560. Go to Tools>Serial Port and select the correct USB connection.

4. If Arduino is running a different program, upload Second_Prototype_Scipt.ino to Arduino.
5. Press control-shift-m to run the script. A command window should appear and say "Waiting for Gamry." (Note: control-shift-m also refreshes to program to the beginning.)
6. Open Gamry Framework. There should be a green circle in the upper-left corner of the program window if the software detects that the Gamry potentiostat is correctly connected to the PC.
7. Open the Sequence Wizard.
8. Load Second_Prototype.GSequence.
9. Make any required changes to the Galvanostatic EIS measurement:
    a. AC current should be 30 microamps.
    b. Set desired frequency range.
    c. Set desired points/decade.
    d. Set file name. The sequence will automatically append "_#X.DTA" to the end of each file, where X is the measurement count. Be careful to change the file name before running a new measurement: not changing the file name may result in data overwriting, although Gamry Framework should warn the user before this can happen.
10. Position probe into sample.
11. Run the sequence from the Sequence Wizard.
12. A window should appear telling the user that a potentiostat has been selected. Press ok if ready for the measurement to start.
13. The measurement should now be in progress. If correctly executed, the Arduino command window should now read "1" to notify the user that the first measurement is in progress.
14. If all measurements were taken successfully, the Arduino command window should now read "Done." The Gamry Framework software should now have a blank screen.
15. Before executing another measurement, press control-shift-m in the Arduino window to refresh the script.

APPENDIX B - SCRIPTS

B.1 Second Prototype Gamry Sequence

Gamry Framework software has the ability to run sequences that allow for easy implementation of looped measurements. The below sequence (Figure 56) loops the Galvanostatic EIS measurement 26 times. The series of Set Digital Out and Delay commands are used to send pulses to the Arduino Mega microcontroller. The below Gamry sequence does not wait from input from the microcontroller: the measurement will commence once the Gamry sequence is executed. This means that the Arduino code should be started first, with the Gamry sequence being executed second (the Arduino code will wait to begin until it receives input from the Gamry sequence).

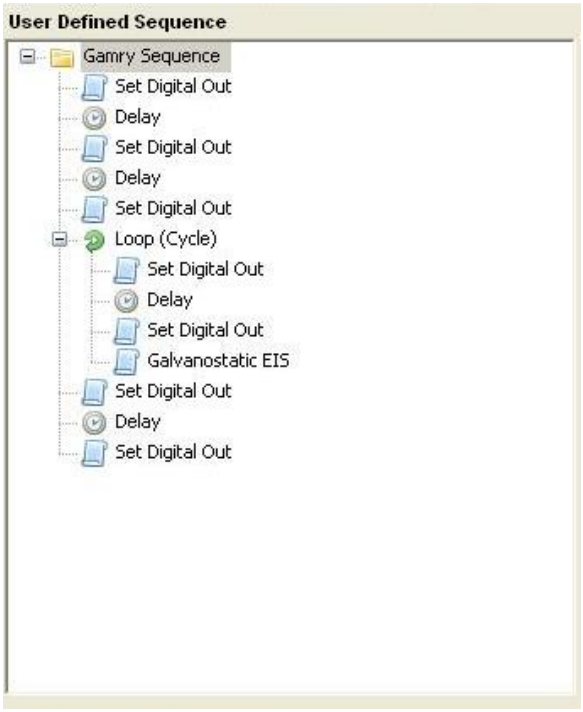

Figure 56: Gamry sequence code for second prototype

B.2 Arduino Code – Second_Prototype_Script.ino

```
//Ryan Snodgrass
//December 2013

const int gam = 23; //INPUT FROM GAMRY
int gam_state = 0; // GAMRY STATE
int j = 1; // LOOP COUNTER

int multiplex [33][6] = {
//A4 A3 A2 A1 A0, switch number for ADG732
{4,4,4,4,4,4}, //dummy row so that array starts at next row (j=1)
{0,0,0,0,0,1},
{0,0,0,0,1,2},
{0,0,0,1,0,3},
{0,0,0,1,1,4},
{0,0,1,0,0,5},
{0,0,1,0,1,6},
{0,0,1,1,0,7},
{0,0,1,1,1,8},
{0,1,0,0,0,9},
{0,1,0,0,1,10},
{0,1,0,1,0,11},
{0,1,0,1,1,12},
{0,1,1,0,0,13},
{0,1,1,0,1,14},
{0,1,1,1,0,15},
{0,1,1,1,1,16},
{1,0,0,0,0,17},
{1,0,0,0,1,18},
{1,0,0,1,0,19},
{1,0,0,1,1,20},
{1,0,1,0,0,21},
{1,0,1,0,1,22},
{1,0,1,1,0,23},
{1,0,1,1,1,24},
{1,1,0,0,0,25},
{1,1,0,0,1,26},
{1,1,0,1,0,27},
{1,1,0,1,1,28},
{1,1,1,0,0,29},
{1,1,1,0,1,30},
{1,1,1,1,0,31},
{1,1,1,1,1,32},
};
```

```
////////////////////////////////////////////////////////////////////////
void setup() {
  Serial.begin(9600);

  pinMode(gam, INPUT);
  for (int i=0; i<=14; i=i+1)
  {
   pinMode(24 + 2*i, OUTPUT);
  }
  for (int i=0; i<=14; i=i+1)
  {
   pinMode(25 + 2*i, OUTPUT);
  }
  //notify user that the program is waiting for input
  Serial.println("Waiting for Gamry.");
  while(gam_state == 0)
  {
    gam_state=digitalRead(gam);
  }
  delay(200);
}
////////////////////////////////////////////////////////////////////////

void loop() {
//wait for input from Gamry
  while(gam_state == 0)
  {
    gam_state=digitalRead(gam);
  }
//notify user of measurement number
  if (j <= 26)
  {
    Serial.println(j);
  }
  else if (j == 27)
  {
    Serial.println("Done.");
    Serial.println(" ");
  }

  // SWITCHING HAPPENS HERE
  if (j <= 13)
  {
    //I  (top, current 1)
    digitalWrite(25,  multiplex[j][4]);
```

```
  digitalWrite(27,  multiplex[j][3]);
  digitalWrite(29,  multiplex[j][2]);
  digitalWrite(31,  multiplex[j][1]);
  digitalWrite(33,  multiplex[j][0]);
  //II (second, voltage 1)
  digitalWrite(35,  multiplex[j+1][4]);
  digitalWrite(37,  multiplex[j+1][3]);
  digitalWrite(39,  multiplex[j+1][2]);
  digitalWrite(41,  multiplex[j+1][1]);
  digitalWrite(43,  multiplex[j+1][0]);
  //III(third, voltage 2)
  digitalWrite(24,  multiplex[j+2][4]);
  digitalWrite(26,  multiplex[j+2][3]);
  digitalWrite(28,  multiplex[j+2][2]);
  digitalWrite(30,  multiplex[j+2][1]);
  digitalWrite(32,  multiplex[j+2][0]);
  //IV (bottom, current 2)
  digitalWrite(45,  multiplex[j+3][4]);
  digitalWrite(47,  multiplex[j+3][3]);
  digitalWrite(49,  multiplex[j+3][2]);
  digitalWrite(51,  multiplex[j+3][1]);
  digitalWrite(53,  multiplex[j+3][0]);
 }
 else if (14 <= j && j <= 26)
 {
  //I  (top, current 1)
  digitalWrite(25,  multiplex[j+3][4]);
  digitalWrite(27,  multiplex[j+3][3]);
  digitalWrite(29,  multiplex[j+3][2]);
  digitalWrite(31,  multiplex[j+3][1]);
  digitalWrite(33,  multiplex[j+3][0]);
  //II (second, voltage 1)
  digitalWrite(35,  multiplex[j+4][4]);
  digitalWrite(37,  multiplex[j+4][3]);
  digitalWrite(39,  multiplex[j+4][2]);
  digitalWrite(41,  multiplex[j+4][1]);
  digitalWrite(43,  multiplex[j+4][0]);
  //III(third, voltage 2)
  digitalWrite(24,  multiplex[j+5][4]);
  digitalWrite(26,  multiplex[j+5][3]);
  digitalWrite(28,  multiplex[j+5][2]);
  digitalWrite(30,  multiplex[j+5][1]);
  digitalWrite(32,  multiplex[j+5][0]);
  //IV (bottom, current 2)
  digitalWrite(45,  multiplex[j+6][4]);
  digitalWrite(47,  multiplex[j+6][3]);
```

```
   digitalWrite(49,  multiplex[j+6][2]);
   digitalWrite(51,  multiplex[j+6][1]);
   digitalWrite(53,  multiplex[j+6][0]);
  }
  while(gam_state == 1)
  {
   gam_state=digitalRead(gam);
  }
  j++; //increase loop counter

}
```

B.3 Post Processing (MATLAB) Code

Code assumes that the .DTA files are in the same directory as the MATLAB script.

Many parameters in the first portion of the code control from which data the tissue image should be generated from and the orientation of the image. The table below is a summary of these parameters.

Table 4: Image generation program parameters

n	Integer	Number of measurements for the loop to read in. Multiple portions of the code will only work correctly with 26 measurements.
base_file_name	String	Provide the base file name of the .DTA files. This is the entire file name before the number and .DTA handle.
freq	Integer	Choose which frequency to plot the image at. 1 is the highest frequency: and subsequent numbers are lower in frequency. This must be manually inspected.
freq_title	String	Also must be manually input. This parameter is the title for the 3D image to be generated.
Data	Character	A, B, D, or E specifies which data to select to graph. A is Zreal, B is Zimaginary,D is Zmod, E is phase.
Num1BR	Binary integer	True makes the first measurement in the bottom right corner. False makes the first measurement in the top left corner.
Loc	String	Another parameter for the title of the 3D graph. Is useful for keeping track of tissue locations.

```
%Ryan Snodgrass
%August 2013 - March 2014

clear all
close all
clc

%%%%%%%%%%%%%%start with reading DTA files

%inputs
n=26; %number of files
base_file_name='2-12-B3_#'; %base file name (the program will automatically
add index to end)
freq=11;                                        %choose frequency
freq_title='100 kHz';
for p=1:n
    current_file_name=[base_file_name num2str(p) '.DTA'];

    fid=fopen(current_file_name);      %file name
    check=' #   s   Hz  ohm ohm V   ohm °   A   V   #'; %read data after this
line
            while 1
                tline = fgetl(fid);
                if ~ischar(tline), break, end %if document ends before
reaching check, end
                TF = strcmp(tline,check); %check for the flag line
                if TF                          %if true, now collect data
                    for i=1:10000
                       tline = fgetl(fid);
                       if ~ischar(tline), break, end
                       temparray=str2num(tline);
                       matrix(i,:)=temparray(1,:);
                       i=i+1;
                    end
                    break
                end
            end
    fclose(fid);

    %%%%%%%% add current matrix to matrices sorted by measurement type
    trans=transpose(matrix);
    a(p,:)=trans(4,:);  %Zreal
    b(p,:)=-trans(5,:); %Zimag
    c(p,:)=(-1)*b(p,:);     %-Zimag
    d(p,:)=trans(7,:); %Zmod
    e(p,:)=trans(8,:); %Zphase in degrees

end
Data=d; %a=Zreal, b=Zimag, d=Zmod, e=phase in degrees
Num1BR=1; %where is the first measurement? true-bottom right, false-top left
Loc='B'; %for liver measurements, which location in tissue?
%
%frequency can be done outside of loop, because it is the same for all
f(1,:)=trans(3,:); %frequency
```

```
%% line plot log
figure(1)
P=Data;
loglog(f,P([1:5],:),'xr'), hold on
loglog(f,P([6:8],:),'xk')
loglog(f,P([9:13],:),'xb')
loglog(f,P([14:18],:),'xr')
loglog(f,P([19:21],:),'xk')
loglog(f,P([22:26],:),'xb')
hold off
xlabel('Frequency (Hz)'), ylabel('Mod Impedance (Ohms)')

%% line plot linear
figure(6)
Fig6=figure(6);
set(Fig6, 'Position', [1300 500 600 500])
P=Data;
%highlight_flag 0 keeps all lines the same color, 1 highlights first three
lines
%line_flag connects (1) or does not connect (0) data points
highlight_flag=0;
line_flag=1;
if (highlight_flag==1 && line_flag==1)
    semilogx(f,P([1:3],:),'-xb'), hold on
    semilogx(f,P([4:26],:),'-xr'), hold off
elseif (highlight_flag==0 && line_flag==1)
    semilogx(f,P([1:26],:),'-xb')
elseif (highlight_flag==1 && line_flag==0)
    semilogx(f,P([1:3],:),'xb'), hold on
    semilogx(f,P([4:26],:),'xr'), hold off
elseif (highlight_flag==0 && line_flag==0)
    semilogx(f,P([1:26],:),'xb')
end

if (Data==e)
    ylim([-90, 10])
end
xlabel('Frequency (Hz)')
if (Data==a)
    ylabel('Real Impedance (Ohms)')
elseif (Data==b)
    ylabel('Imag Impedance (Ohms)')
elseif (Data==d)
    ylabel('Mod Impedance (Ohms)')
elseif (Data==e)
    ylabel('Phase (Degrees)')
end

xlim([1E3 1E5])
%% 2d contour
thousand=Data(:,freq);
thousand=thousand';
t(1,[1:13])=thousand(1:13);
t(2,[1:13])=thousand(14:26);

figure(2)
```

```
contourf(t,2), hold on
title(' ')
hFig=figure(2);
set(hFig, 'Position', [600 100 1300 150])
set(gca,'YTick',[])
set(gca,'XTick',[1:13])
for i=1:13
    for j=1:2
        plot(i,j,'ok','Markersize',8,'MarkerFaceColor','y')
    end
end
hold off
xlabel('Measurement Position')
c2=colorbar;
if (Data==a)
    title(c2,'Z_{real} (Ohms)')
    elseif (Data==b)
    title(c2,'Z_{imag} (Ohms)')
    elseif (Data==d)
    title(c2,'Z_{mod} (Ohms)')
    elseif (Data==e)
    title(c2,'Phase (Degrees)')
end
%% bar plot

single_f=Data(:,freq); %selects data of a single frequency
%split data to two rows
if Num1BR==1
    single_data(1,[1:13])=single_f(26:-1:14);
    single_data(2,[1:13])=single_f(13:-1:1);
else
    single_data(1,[1:13])=single_f(1:13);
    single_data(2,[1:13])=single_f(14:26);
end
figure(5)
if (Data==e)
    single_data=-1*single_data;
    h=bar3((single_data));
else
    h=bar3((single_data));
end
h=bar3((single_data));
Fig=figure(5);
set(Fig, 'Position', [50 200 600 600])
pbaspect([8 2 4])
title(['Location ' Loc 10 'Input: 30 µA at ' freq_title 10 'Measurement
Pitch: 1.27 mm'],'FontSize',14,'FontWeight','bold')
if (Data==a)
    zlabel('Z_{real} (Ohms)','FontSize',14,'FontWeight','bold')
    elseif (Data==b)
    zlabel('Z_{imag} (Ohms)','FontSize',14,'FontWeight','bold')
    elseif (Data==d)
    zlabel('Z_{mod} (Ohms)','FontSize',14,'FontWeight','bold')
    elseif (Data==e)
    zlabel('-Phase (Degrees)','FontSize',14,'FontWeight','bold')
end
set(gca,'FontSize',14,'fontWeight','bold')
```

```
set(findall(gcf,'type','text'),'FontSize',14,'fontWeight','bold')

if Num1BR==1
    set(gca,'XTickLabel',{[13:-1:1]})
    set(gca,'YTickLabel',{[2:-1:1]})
else
    set(gca,'XTickLabel',{[1:1:13]})
    set(gca,'YTickLabel',{[1:1:2]})
end

view(35,25)
c=colorbar;
if (Data==a)
    title(c,'Z_{real} (Ohms)','FontSize',14,'FontWeight','bold')
    elseif (Data==b)
    title(c,'Z_{imag} (Ohms)','FontSize',14,'FontWeight','bold')
    elseif (Data==d)
    title(c,'Z_{mod} (Ohms)','FontSize',14,'FontWeight','bold')
    elseif (Data==e)
    title(c,'-Phase (Degrees)','FontSize',14,'FontWeight','bold')
end

for k = 1:length(h)
    zdata = get(h(k),'ZData');
    set(h(k),'CData',zdata,...
             'FaceColor','flat');
end
```